Chapter 4

Cyclic Flame Propagation in a Fully Premixed Initially Stagnant Mixture

4.1 Introduction

This chapter focuses on the periodic flame motion, the puffing flame described in Chapter 3, that was discovered during the investigation of flame propagation subsequent thermal ignition.

Flames exhibiting a flickering or puffing behavior with frequencies around 10 Hz have been discussed since the First International Symposium on Combustion in September 1928 (Chamberlin and Rose, 1948). The oscillation of non-premixed gaseous flames were investigated experimentally by Kimura (1965), Toong et al. (1965), Grant and Jones (1975), Durao and Whitelaw (1974), and later by and Tanoue et al. (2010). Theoretical work has been carried out by Buckmaster and Peters (1988), who investigated oscillations associated with the model problem of an infinite candle. Similar oscillations have also been observed in fires above pools of liquid fuels (Cetegen and Ahmed, 1993) and in room fires (Zukoski, 1986).

These oscillations are not limited to non-premixed flames, but can also occur in premixed flames as shown by Strawa and Cantwell (1989), Durox et al. (1990), Kostiuk and Cheng (1995), Cheng et al. (1999), Shepherd et al. (2005), and Guahk et al. (2009). In these studies, the frequency of the motion is also on the order of 10 Hz. In all of the previous experiments of premixed flames, the gaseous mixture was injected into the burner at a specific injection velocity. In contrast, the experiments and simulations presented here are performed in a combustible mixture, which is quiescent prior to the ignition sequence. The following investigation of the cyclic flame propagation in a premixed environment is conducted using a combined experimental and numerical approach.

4.2 Experiments

4.2.1 Experimental Setup and Procedure

The experimental setup and procedure for the cyclic flame propagation are the same as used in the study of hot surface ignition detailed in Chapter 3, with a few additions. Experiments are performed using a standard diesel glow plug (Autolite 1110), a high-temperature glow plug (noncommercial Bosch 978801-0485), as well as a nickel foil, and a chromel wire in order to investigate the effect of the hot surface size. The characteristic dimensions of the different hot surfaces, as well as their power consumptions are given in Table 4.1. Similarly, two vessels of different sizes, the 2 liter vessel shown in Figure 3.1 and a 22 liter cylindrical vessel, are used to test the effects of vessel size and recirculation. The cyclic or puffing flame is visualized using either a regular z-type schlieren system showing the density gradients (Figure 4.1), or by observing the excited CH radical, CH^* (Figure 4.2), which is created in the combustion of hydrocarbon fuels at the flame front.

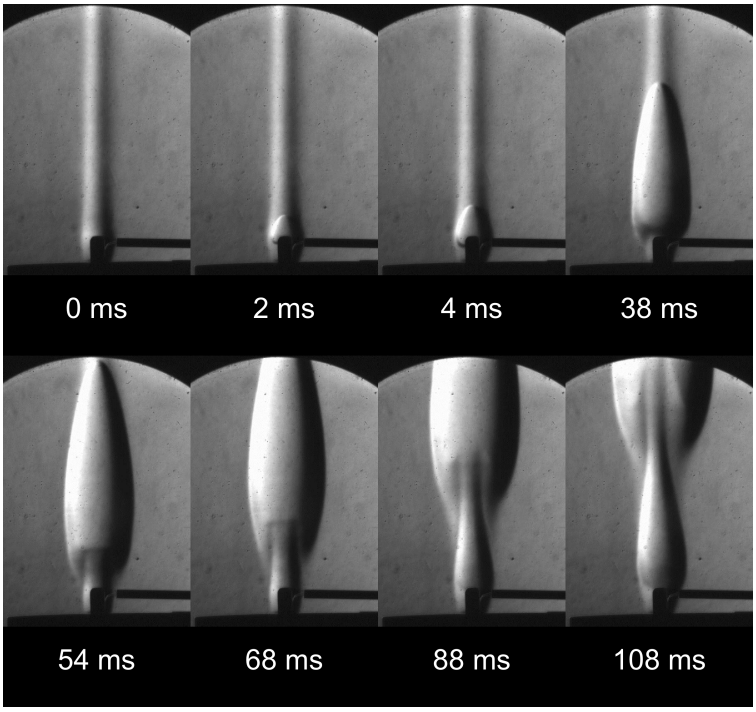

Figure 4.1: Schlieren images of ignition and subsequent flame propagation in a mixture of hexane in air at atmospheric pressure ($\phi = 3.0$). The hot surface is an Autolite 1110 glow plug, mounted in a 60-mm-diameter aluminum cylinder in a closed 22 liter combustion vessel. The hot surface temperature is measured by a fine wire K-type thermocouple at the hottest point on the glow plug.

The images of CH^*, which emit light between 420 and 440 nm, are acquired by observing the flame directly through a narrow bandpass filter (center wavelength $\lambda_c = 450\pm10$ nm, 70 ± 30 nm

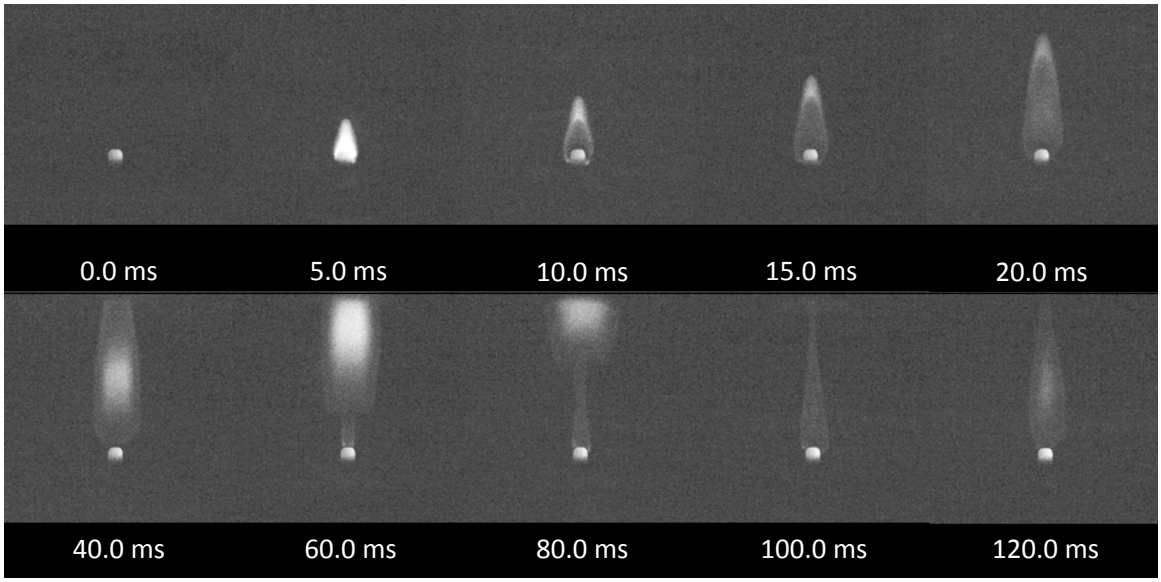

Figure 4.2: Direct imaging of CH* molecules through a bandpass filter (λ_c = 460 nm with FWHM 40 nm) and a short-pass filter (transmittance > 75% in the range of λ = 430–500 nm), ϕ = 3.0

FWHM) and a short-pass filter (transmittance > 75% in the range of λ = 430–500 nm). Figure 4.3 gives the transmittance curve of the combined optical filter and the CH* emission spectrum. Due to the low light level, the exposure time is increased to 5 ms and the frame rate is reduced to 200 frames per second. Afterwards, the contrast of the images is enhanced in order to the make the flames more easily visible.

4.2.2 Experimental Observations

The usual combustion mode following ignition in a closed vessel is a singe quasi-spherical flame that spreads in all directions, and is distorted by buoyancy at low propagation velocities (i.e., very lean or rich mixtures). As described in Chapter 3, the hot surface establishes a thermal buoyant plume in the vessel, which induces an initial flow field prior to ignition. This thermal plume is shown in the first schlieren image in Figure 4.1 for a rich *n*-hexane-air mixture (ϕ = 3.0). Then, the mixture ignites near the tip of the glow plug and propagates quickly upward along the thermal plume. At this equivalence ratio, the laminar burning velocity is very low – around 20 cm/s (see Figure 3.31). Due to the temperature increase within the plume and the buoyancy-induced flow, the upward flame propagation velocity is significantly higher than the flame propagation velocity on the sides. In the schlieren images, the flame appears not to propagate downward after ignition due to the upward flow velocity at the glow plug base. As subsequently shown by numerical simulations, the upward

velocity is induced initially by the thermal plume of the glow plug and subsequently by buoyancy and vorticity produced by the combustion products.

Once ignition has occurred, the temperature in the region above the hot surface is determined by combustion products. The upward motion of the buoyant hot products entrains cold premixed, but unreacted, gas. The entrainment velocity limits the horizontal spreading of the flame. The puffing behavior appears to be a result of the instability of the flow and the flame sheet due to the interaction between the entrainment, buoyancy-induced flow, and flame dynamics. Following the initial ignition transient, the temperature distribution and flow field is determined by the continuous, but periodically varying, cylindrical flame extending upward from the thermal ignition source. Radial entrainment provides a continuous source of fresh reactants. The resulting configuration appears to be an axisymmetric "V-flame" anchored by the ignition source.

The sequence of images showing the CH^* luminescence in Figure 4.2 further illustrates the puffing phenomenon. In the images three different sources of light are visible: CH^* radiation, which is produced at the flame front; second the tip of glow plug, which radiates over a broad spectrum; and finally soot, visible in the middle of the flame at later times, which also radiates over a broad spectrum. This technique is not sensitive to density gradients, so the initial plume is not visible. In the second image, ignition at the top of the glow plug is clearly visible. The flame propagates outward, more quickly within the hot plume above the glow plug, but remains a continuously connected flame and anchored at the top of the glow plug.

The puffing process occurs at a consistent frequency of about 6-15 Hz depending on the initial composition. The scaling of the puffing frequency and the physics of the puffing phenomenon are examined in detail in the following sections.

4.2.3 Numerical Simulations [1]

Two-dimensional unsteady simulations are performed using the same flamelet model as described in Chapter 3. Ignition is simulated by creating a small spherical flame sheet at the top of the glow plug inside the established thermal plume. The initial thermal plume created while the glow plug heats up to ignition temperature (as discussed previously) was simulated in order to have a realistic comparison of experimental and computational results.

Simulations are performed for both glow plug geometries (Bosch and Autolite - see Sections 3.2.3 and 3.2.4), resulting in puffing flames over a range of n-heptane-air mixtures from $\phi = 2.5$–3.0 with

[1] All numerical simulations were performed by Shyam Menon and Guillaume Blanquart

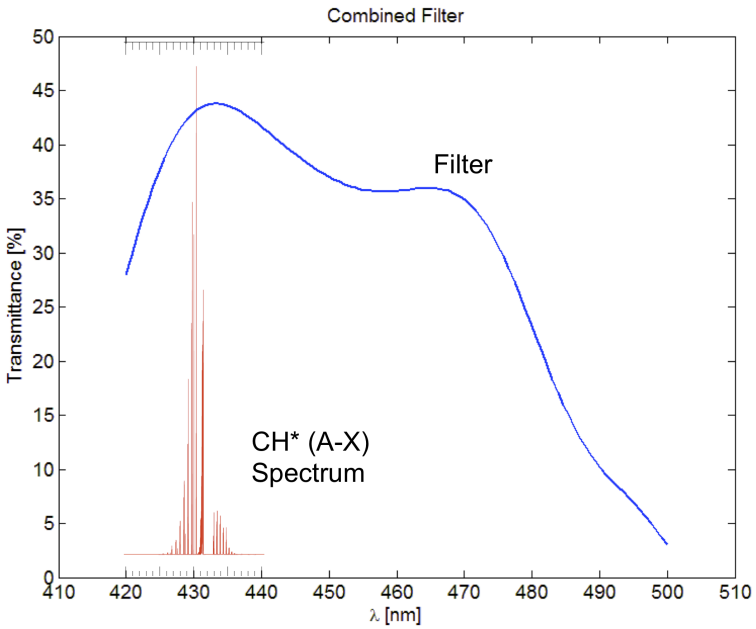

Figure 4.3: Transmission curve of the combined filter and CH* spectrum calculated with LifBase (Luque and Crosley, 1999) superposed on the filter transmission function

small variations in the puffing frequency. The simulations, such as the one in Figure 4.4, show the flame propagating outward initially before the deformation of the flame front develops as observed in the experiments. Once it was demonstrated that the simplified numerical model gave realistic results, it was used to explore the effect of a variety of parameters as well as the details of the flow field.

4.3 Results — Puffing Frequency

As seen in the previous chapter, the combustion mode depends on the exact composition of the mixture and possibly other factors such as size of the hot surface. The effect of total vessel volume is of special interest because for very small vessel sizes the combustion products could force the flow into a large-scale recirculation or result in coupling to the acoustic modes with the flame motion. The following section provides details on the effects of these parameters and gives dimensional arguments on how the frequency changes as function of the flame propagation speed and gravity.

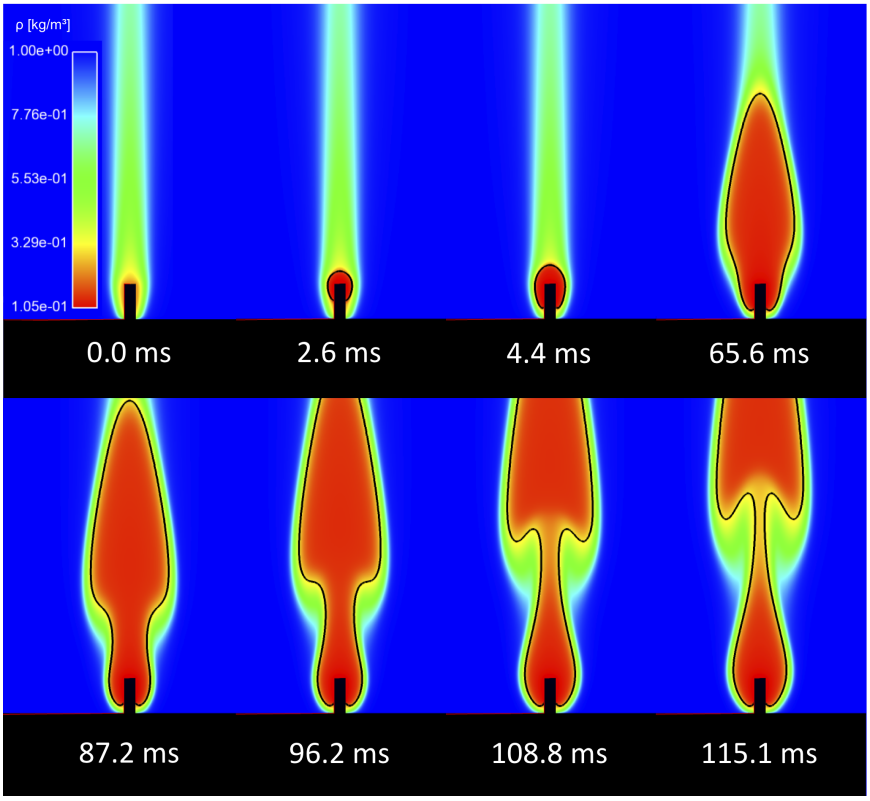

Figure 4.4: Simulation results (density contours) for flame propagation phenomena at an equivalence ratio of $\phi = 2.5$. The black line represents the location of the flame front as marked by the iso-contour of the progress variable, $C = 0.15$.

4.3.1 Glow Plug Size and Vessel Size

The experiments were performed with 4 different heat sources as listed in Table 4.1. The measurements show that there is a very limited dependence of the puffing frequency on igniter size, as well as power input. Similarly, changing the vessel volume from 2 to 22 liters did not change the puffing frequency noticably. Similar analysis is performed with numerical simulations by changing the size of the modeled glow plug by a factor of 0.5 and 2 and the size of the vessel from 1 liter to 5 liters[2]. These observations suggest that the frequency is a function of the flame dynamics and the flow induced by the flame, and is independent of the igniter and vessel sizes. This rules out that the periodic motion is caused by a recirculation created by the flame pushing the unburned gas upward stagnating at the top, pushing fluid down the side and back into the flame. The independence of frequency from vessel size also rules out acoustic interactions with the enclosure as a possible puffing mechanism.

[2]The numerical simulation only models the vessel above the stagnation surface, which is roughly in the middle of the vessel giving a volume of 1 liter for small vessel. The large vessel is only modeled to a size of 5 liters to limit the number of grid points and the computational time required.

Table 4.1: Puffing behavior for fuel-rich hexane air mixture ($\phi = 3.0$)

Hot Surface	Power [W]	Area [m^2]	V_{vessel} [m^3]	T_{ign} [K]	Freq. [Hz]
Bosch Glow Plug†	≈100	8×10^{-5}	2×10^{-3}	920-975	12-13 (+1/-1)
Autolite 1110 Glow Plug	96	1.5×10^{-4}	2×10^{-3}	775-825	12-13 (+1/-2)
			22×10^{-3}	1120	14-15 (+1/-1)
Nickel Foil 0.05 mm	≈400	2.4×10^{-5}	2×10^{-3}	980	20 (+8/-2)
Chromel Wire ⌀ 0.13 mm	≈10	2.4×10^{-6}	2×10^{-3}	n/a	14 (+3/-2)

† non-commercial Bosch (961) 64 978801-0485 Duraterm
n/a - not available

4.3.2 Scaling Laws

4.3.2.1 Cetegen and Ahmed (1993)

Buoyant plumes and pool fires have instabilities and periodic motions that are very similar to those observed in the present premixed puffing flames. As a first approximation, the frequency behavior of plumes and pool fires can be estimated using dimensional analysis. The observed frequency is a function of the buoyancy-induced flow, with no puffing was observed in zero-g conditions[3], making gravity, g, one of the parameters of interest. The main length scale parameter is the diameter of the burner, D, through which either a buoyant plume of light gas, such as helium, combustion products from a preburner, or a pool of evaporating fuel is introduced. Cetegen and Ahmed (1993) suggest that the following nondimensional ratio

$$\frac{f^2 D}{g} \tag{4.1}$$

has a universal value. This implies that at a constant gravitational acceleration,

$$f \sim D^{-1/2} \, . \tag{4.2}$$

Cetegen and Ahmed (1993) compiled data for many different gaseous and liquid fuels as well as light gases and showed good agreement using this scaling argument for burner sizes of approximately 10^{-2} to 10^{1} m.

For pool fires, the size of the pool determines the size of the flame. The fuel from the liquid or gaseous pool has to mix with the air outside to create a combustible mixture. This mixing interface originates near the edge of the fuel pool. The diameter of the flame, d_f, is therefore fixed and proportional to the pool diameter as shown in Figure 4.5.

[3]Simulations of the configuration shown in Figure 4.4 were performed without gravity (Menon, 2011).

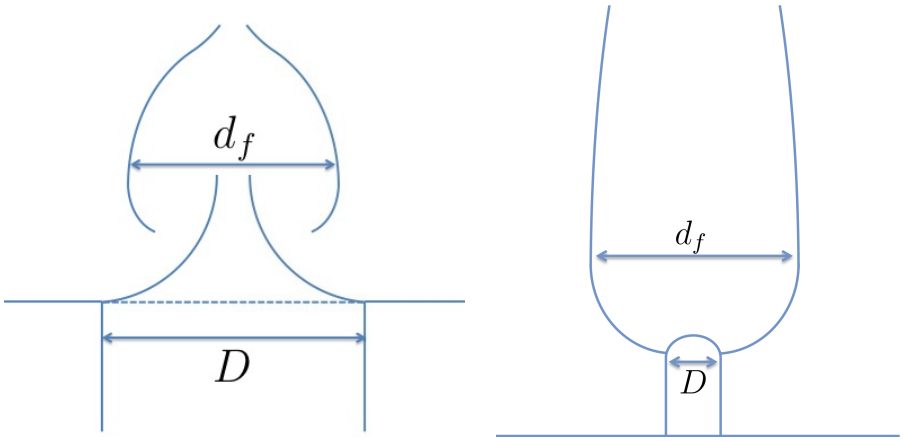

(a) (b)

Figure 4.5: (a) Flame diameter, d_f and pool diameter, D, based on Cetegen and Ahmed (1993). (b) Flame diameter, d_f and hot surface, D, for premixed puffing flames

$$d_f \propto D \tag{4.3}$$

The puffing flames described here, however, are premixed flames. The diameter of the flame significantly exceeds that of the hot surface since the flame starts at the hot surface and propagates outward until the flame front becomes unstable and the upward flow sweeps it away. The flame initially propagates outward spherically so that the radius scales as $\epsilon S_{l,u} t$, where ϵ is the density ratio across the flame front and $S_{l,u}$ is the laminar flame speed relative to the unburned gas [4]. The flame diameter increases until the instability takes over, giving the time scale of $T \sim 1/f$. We propose that the characteristic diameter of the flame can be modeled as the sum of the two terms,

$$d_f = 2\frac{\epsilon S_{l,u}}{f} + D\ . \tag{4.4}$$

The first term represents the diameter of the flame at the peak of the puffing cycle and the second term represents the diameter of the hot surface, D, the initial position from which the flame starts.

In the present experimental study, hot surfaces with different diameters, ranging from $D =$ 0.1 mm to $D = 5$ mm were considered. The puffing period, T, is about 0.1 s for flame propagations speeds of about 0.2 m/s. Under these conditions, the flame diameter changes by only 12.5% for a change in hot surface size of almost 2 orders of magnitude. If as an initial approximation the diameter of the hot surface is neglected, a new nondimensional ratio can be formulated similar to

[4] In this thesis $S_{l,u}$ and S_l are used interchangeably to mean the laminar flame speed relative to the unburned gas.

the one proposed by Cetegen and Ahmed (1993) in Equation 4.1

$$N_B = \frac{f\epsilon S_{l,u}}{g} = \frac{\epsilon S_{l,u}}{gT} \ , \tag{4.5}$$

has a value of 0.2-0.3, which is comparable 0.23 found by Cetegen and Ahmed (1993) [5].

$$f \propto g \text{ for fixed } \epsilon S_{l,u} \tag{4.6}$$

and

$$f \propto (\epsilon S_{l,u})^{-1} \text{ for fixed } g \ . \tag{4.7}$$

These scaling results are compared with experimental data in the subsequent sections.

4.3.2.2 Durox et al. (1996)

Durox et al. (1996) investigated the the flickering of jet diffusion flames and arrived at a different set of scaling relations. Fuel is introduced through a small nozzle (2–4 mm in diameter) at low velocities (2 mm/s). Tests were performed at varying pressure and at varying gravitational acceleration, which was achieved during parabolic flight tests. In these experiments, the mean diameter of the flame is greater than the nozzle diameter. In contrast, in pool fire experiments, the mean flame diameter is smaller than the pool diameter.

Through dimensional analysis the frequency, f, is scaled with the gravitational acceleration, g, and the viscous diffusion, ν,

$$f^3 \sim \frac{g^2}{\nu} \ . \tag{4.8}$$

Durox et al. (1996) perform a more detailed theoretical analysis of the flame instability, where the flame creates a constant inflow of hot gases in the middle and thus a shear layer is formed across the flame front. Durox et al. argue that the most amplified frequencies, f, in this flow are given by

$$f = c\left[\left(\frac{\rho_u - \rho_b}{\rho_b}\right)^2 \frac{g^2}{\nu_b}\right]^{2/3} \tag{4.9}$$

where c is a constant, ρ_u and ρ_b are the unburned and unburned density, g is the gravitational acceleration, and ν_b is the viscosity of the burned gas. This scaling is based on the developments of the instabilities at a certain height above the nozzle exit, but can also be obtained by dimensional

[5] Cetegen and Ahmed (1993) give the scaling for pool fires at normal gravity as $f = 1.5D^{-1/2}$. Squaring both sides and dividing through by g gives $(f^2D)/g = 0.23$.

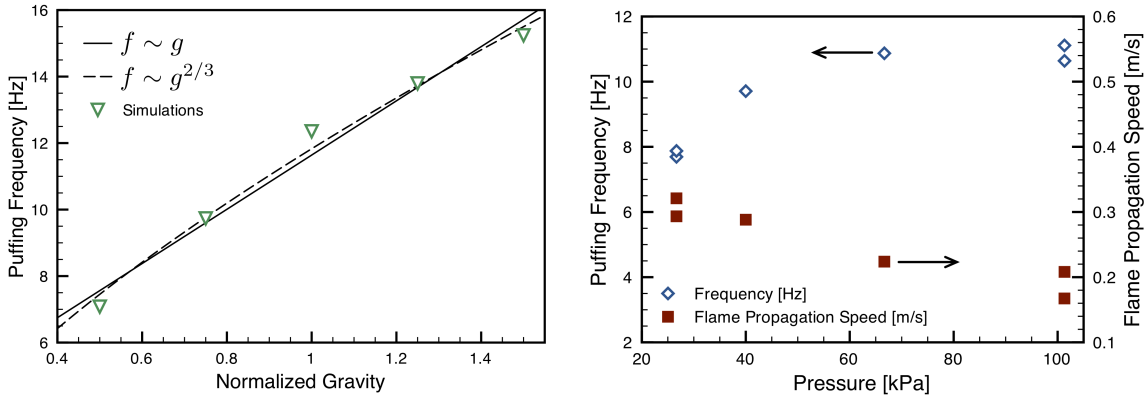

(a) (b)

Figure 4.6: (a) Simulation results for the puffing frequency as a function of gravitational acceleration. (b) Experimental results for puffing frequency and flame propagation speed as function of initial pressure at $\phi = 2.5$

analysis when considering only the effects of buoyancy acceleration [m/s^2] and kinematic viscosity [m^2/s]. As the viscosity varies with pressure as $\nu_b \sim P^{-1}$ (Durox et al., 1996) the frequency can be written as

$$f \propto g^{2/3} \text{ and } f \propto P^{1/3} . \tag{4.10}$$

Note that this model predicts that the frequency is dependent on viscosity rather than burning speed because the combustion is not premixed. This scaling will be compared to the experimental data and the ideas of the previous section in the next section.

4.3.3 Effect of Gravity

In the puffing flames described here, the flame front initially spreads out from the hot surface almost spherically, with a propagation speed equal, V_f, that is close to the product of the expansion ratio, ϵ, and the laminar burning speed relative to the unburned gas, $S_{l,u}$. Gravity creates a buoyancy force on the burned gas, which is less dense than the surrounding gas, and lifts the flame upward once it has reached a critical size. The burned gas moves upward more rapidly than it is replenished by combustion of inward flowing combusted gas. This process appears to be responsible for the puffing behavior and gives rise to the characteristic frequency. Experiments and simulations confirm that the frequency of the puffing changes with the flame propagation speed and magnitude of gravitational acceleration.

Figure 4.6 (a) shows the results of a computational study of changing the acceleration of gravity. With increasing values of g, the puffing frequency increases. This is consistent with the flame puff being lifted by the acceleration of gravity and the hydrostatic pressure, creating an entrainment flow pinching the flame together. Both of these effects are increased as the acceleration due to gravity is increased.

Over the range investigated both the linear relation, $f \sim g$, as well as the nonlinear relation, $f \sim g^{2/3}$ are both consistent with the simulation results. The nonlinear scaling gives a zero puffing frequency at zero gravitational acceleration, which is expected from the postulated mechanism and simulations. The y-intercept of the linear scaling is not zero, which can be attributed to the initial diameter of the flame being neglected. This indicates that a more general relationship for scaling should be considered, which is done in the next section.

4.3.4 Effect of Flame Speed

The flame propagation speed can be varied in the experiments by either changing the initial pressure of the mixture or changing the composition. In Figure 4.6 (b), experimental results are shown for varying the initial pressure from 25 to 100 kPa for a $\phi = 2.5$ n-hexane/air mixture. As the pressure is decreased from ambient, the measured flame propagation speed increases, which is consistent with other data on slow burning flames Lewis (1954), Gaydon and Wolfhard (1979), Kelley et al. (2011), and the puffing frequency decreases.

A re-analysis of the relationship above is shown in Figure 4.7. The puffing period, $T = 1/f$, is plotted versus the flame propagation speed for both experiments and simulations. The experimental mixtures shown are n-hexane in air from $\phi = 2.15-3.0$ and at initial pressures varying from 25 kPa to 100 kPa, 7% and 8 % hydrogen in air, as well as lean and rich hexane mixtures doped with hydrogen (see the following section). In agreement with the proposed scaling relationship, the puffing period increases approximately linearly with flame speed for all experimental and computational results. The deviation from a linear relationship can be rationalized as being due to neglecting the initial hot surface diameter (D) in Equation 4.4. The zero flame speed intercept has a finite puffing frequency that is consistent with the plume and pool fire scaling proposed by Cetegen and Ahmed (1993).

A more general expression may be derived by using the full form of Equation 4.4. Following the arguments from Cetegen and Ahmed (1993), and assuming that the important length scale is the

diameter of the hot products, we propose that the following expression must be a constant:

$$\frac{f^2 d_f}{g} = \frac{2\epsilon S_{l,u} f}{g} + \frac{f^2 D}{g} = \text{constant} = C \ . \tag{4.11}$$

We can rearrange this equation to give

$$\epsilon S_{l,u} = \frac{gC}{2} T - \frac{kD}{2} \frac{1}{T} \tag{4.12}$$

where the flame propagation speed is a function of the puffing period as plotted in Figure 4.7 which can be written as a quadratic equation for the puffing period

$$\frac{gC}{2} T^2 - \epsilon S_{l,u} T - \frac{kD}{2} = 0 \ . \tag{4.13}$$

An additional constant k has been introduced to provide a better fit to the experimental data and account for the fact that the initial flame diameter may not be exactly D. Using all experimental and numerical results, the coefficients C and k were found using a least squares minimization ($C = 0.64$ and $k = 3.35$).

Figure 4.7 shows both the experimental data and simulation results. The linear relation, ($k = 0$) is also shown; while in general agreement with the observations, the nonlinear correlation (4.12) is a definite improvement.

A direct comparison with the scaling proposed by Cetegen and Ahmed (1993) is also possible by setting the flame speed to zero. In dimensional form, the frequency in Hz as function of diameter in meters at 1 g is given by Cetegen and Ahmed (1993) as

$$f = 1.5 \, D^{-1/2} \ . \tag{4.14}$$

Setting $S_{l,u} = 0$ in Equation 4.12 results in expression

$$T = \sqrt{\frac{gC}{k}} D^{-1/2} \tag{4.15}$$

Using the results obtained for the coefficients C and k, the constant of proportionality is $\sqrt{gC/k} = 1.4$ Hz m$^{1/2}$, which is within 10% of the Cetegen and Ahmed value.

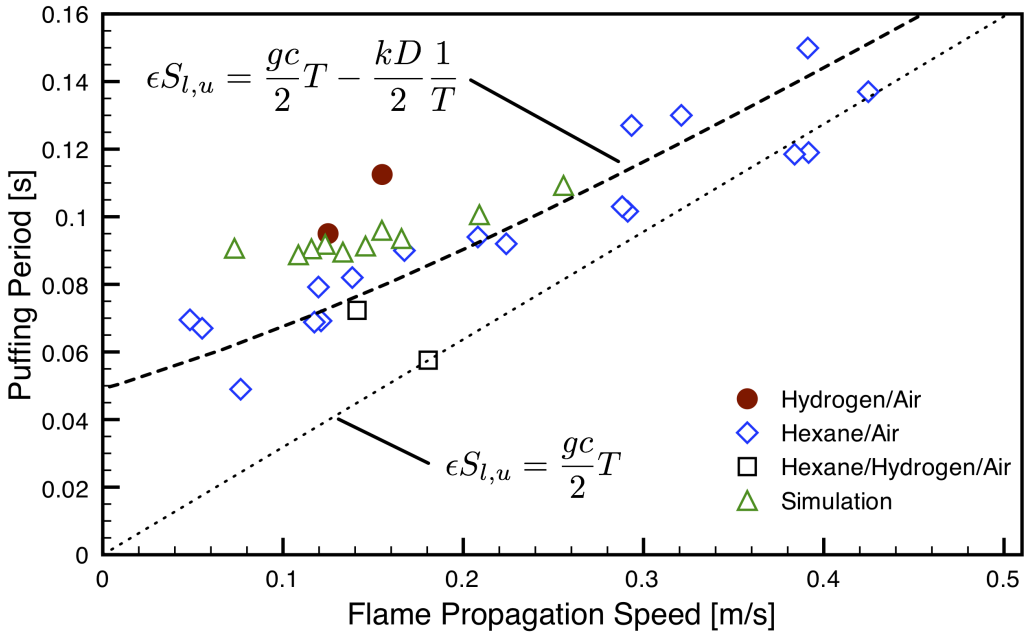

Figure 4.7: Puffing period vs. horizontal flame propagation speed for n-hexane air mixtures from ϕ = 2.15–3.0, 7% and 8% hydrogen in air and hexane/hydrogen/air mixtures at atmospheric pressure

4.3.5 Lean Hexane Puffing Flames [6]

Based on the scaling ideas presented above, the phenomenon of puffing flames should not be limited to rich hydrocarbon mixtures, but should also occur in lean hydrocarbon mixtures if the flame speed is sufficiently slow. However, tests using lean hexane-air mixtures did not show puffing, apparently because the lower flammability limit is reached in the experiments before the flame propagation speed is sufficiently slow.

We were able to show that the puffing phenomenon does occur in lean hydrogen flames. In hydrogen flames, much lower flame speeds can be obtained with lean mixtures than in *n*-hexane-air cases. For lean H_2-air mixtures, the flame speed gradually increases as hydrogen concentration is increased, and for rich mixtures, the flame speed changes quickly with increasing concentration until the upper flammability limit is reached. Hydrogen-air mixtures have a very wide range of flammability from 4% to 75% (Zabetakis, 1965). Lean puffing hydrogen flames were observed for 7% and 8% hydrogen in air at frequencies or 10.5 and 8.9 Hz, respectively. For a 5% mixture only a single puff is visible, which propagates upward and the flame extinguishes. Figure 4.8 shows the flame speed as a function of hydrogen mole fraction from current experiments and simulations performed by Bane (2011).

[6] This work was presented by Brian Ventura in his senior thesis in May 2011

We can take advantage of the wide flammability range and slow flame speed of lean hydrogen-air mixtures by adding small amounts of hydrogen to hexane-air mixtures just below the flammability limit. Adding hydrogen to a mixture of n-hexane-air, which is below the flammability limit makes it possible to ignite the mixture and obtain slow flame speeds. Figure 4.8 shows flame speeds from experiments and simulation of n-hexane-air mixtures whose lowest propagation speed is just above 30 cm/s. Initially this increases the propagation speed as shown by the mixtures of 1.1% n-hexane and 2% hydrogen in Figure 4.8. However, decreasing the amount of hydrogen and n-hexane reduces the flame propagation speed to 25 cm/s, which leads to a series of puffing flames. The mixture of 1.05 % n-hexane and 1.5 % hydrogen (highlighted in Figure 4.8) has sufficiently a slow flame propagation speed that and shows a puffing flame at $\sim$ 17 Hz (see shot 123).

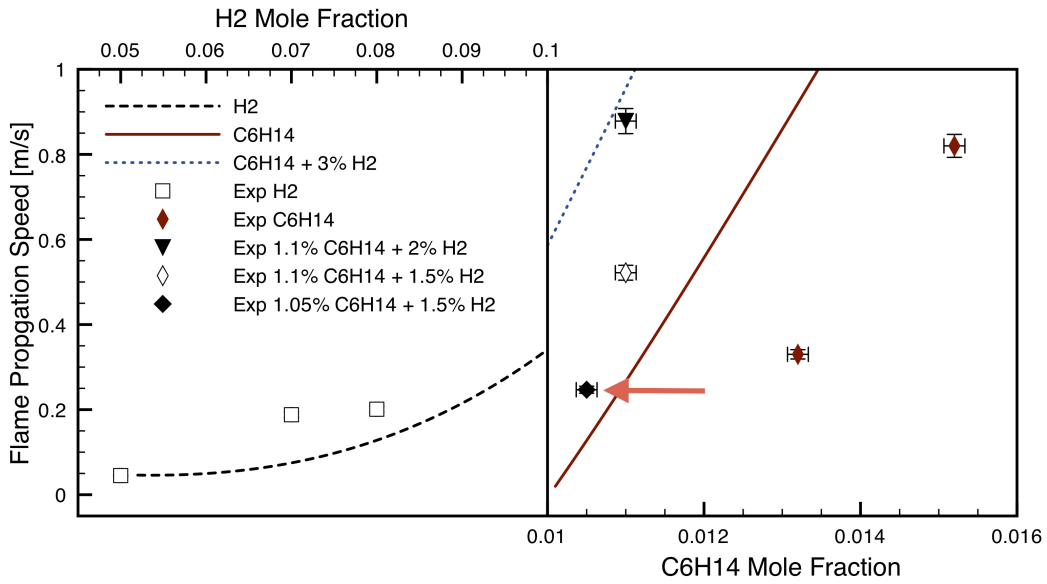

Figure 4.8: Flame propagation speeds of hydrogen-air, n-hexane-air, and hydrogen-n-hexane-air mixtures at atmospheric pressure

4.4 Physics of Puffing

Experiments and simulations have both demonstrated a periodic motion associated with flame propagation in rich premixed hydrocarbon-air mixtures (and lean hydrogen flames). We have also verified that the frequency of this periodic motion is linked to the flame propagation speed and acceleration due to gravity. The instability of the flow and flame front leading to the periodic motion apparently arises from a competition between flame propagation and buoyancy-induced entrainment flow with additional effects from volumetric expansion and vorticity. In order to get more insight into the puffing mechanism, the simulation results are used to analyze the instantaneous flow field associated with the combustion-induced flow as well as the generation of vorticity by the flame and boundaries.

4.4.1 Flow Field Analysis

The flow field is created by three different effects resulting from the combustion process. Across the flame, the temperature is increased, which lowers the density inside the flame. This volumetric expansion across the flame front induces a dilatation flow field ahead of the flame front because the flow is subsonic. The lighter gas inside the flame is also accelerated upward by buoyancy, creating an entrainment flow at the bottom of the flame. At the flame front, vorticity is created, predominantly from baroclinic torque arising from the misalignment of the density gradient across the flame front and the hydrostatic pressure gradient. The inflow created by the motion of the flame and the hot products opposes the flame propagation at the bottom of the flame.

Part of the effect of the dilation produced by combustion can be estimated by treating the flame as an ideal cylindrical flame. In Section 3.5.2 the flame propagation speed of a spherically expanding flame is estimated using a mass balance across the flame front. The result for a cylindrical flame or radius R with stationary combustion products is

$$\dot{R} = \epsilon S_l \tag{4.16}$$

where $\dot{R}$ is the expansion rate of the flame, ϵ is the density ratio across the flame front, and S_l is the laminar burning speed. The definition of the burning speed is the speed at the which the flame propagates relative to the underlying flow velocity u,

$$S_l = \dot{R} - u(R) \; . \tag{4.17}$$

For incompressible, cylindrical flow the mass conservation outside the flame gives the velocity at any location $r > R$ in terms of the velocity $u(R)$ just ahead of the flame flame

$$\rho_u U(R) 2\pi R(t) = \rho_u u(r) 2\pi r \tag{4.18}$$

$$u(r) = U(R)\frac{R(t)}{r} = (\epsilon - 1)S_l \frac{R(t)}{r} \quad \text{for} \quad r \geq R \tag{4.19}$$

with the assumption that the flow inside the flame is stationary, $u = 0$ for $0 \leq r < R$. For spherical flames, a similar derivation gives

$$u(r) = (\epsilon - 1)S_l \frac{R^2(t)}{r^2} \quad \text{for} \quad r \geq R\,. \tag{4.20}$$

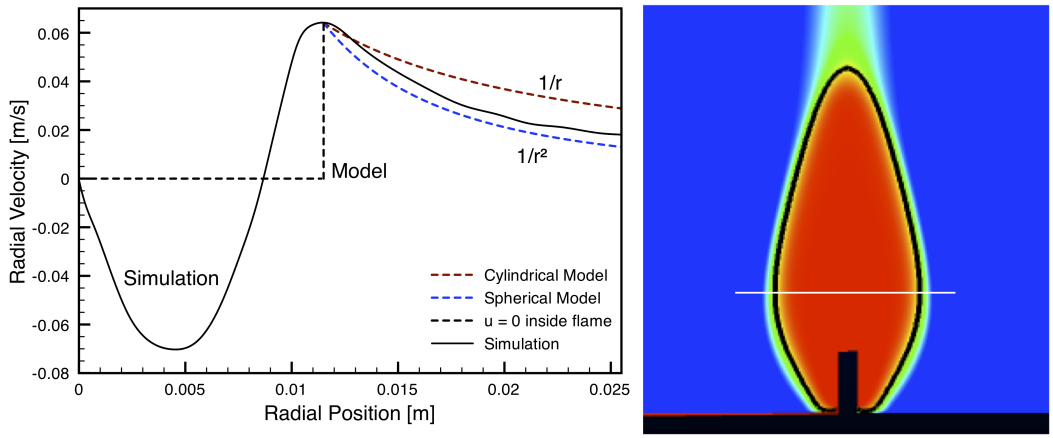

(a) Velocity profile along the radial direction

(b) Simulation at 50 ms

Figure 4.9: Radial velocity profile

Figure 4.9 (a) shows the radial velocity as a function of radial position from simulation at the widest part of the flame at 50 ms as indicated in Figure 4.9 (b). The simulations show that inside the flame, we have nonzero flow towards the center. This is not captured by the simple model and is due to the upward accelerating flow due to buoyancy and vorticity. Outside the flame, the flow is outward and the variation with radius is between r^{-1} and r^{-2} depending on the distance from the flame. The induced outward flow opposes the inflow leading to the formation of a puff, as discussed in the next section. Since the flow is nonzero inside the flame, we cannot use the simple models to achieve a good estimate of the flow velocity produced by the volumetric expansion across the flame front.

An alternative estimate of the influence of the volumetric expansion can be obtained by comput-

ing the pressure jump across the flame. In the reference frame of the flame, the unburned gases flow into the flame at a speed, w_1, the laminar burning speed, and exit the flame at the flame propagation speed, w_2, the product of laminar burning speed and the expansion ratio.

$$w_1 = S_l \tag{4.21}$$

$$w_2 = \epsilon S_l \tag{4.22}$$

The jump relation across the flame front is

$$P_2 + \rho_2 w_2^2 = P_1 + \rho_1 w_1^2 \, , \tag{4.23}$$

where the subscript 1 represents unburned gas and subscript 2 represents burned gas. Substituting in for the velocities and densities gives

$$P_2 - P_1 = \rho_u \left(S_l^2 - \frac{\rho_b}{\rho_u} \epsilon^2 S_l^2 \right) \, , \tag{4.24}$$

with $\epsilon = \rho_u / \rho_b$ this results in the pressure jump being

$$\Delta P = -\rho_u S_l^2 (\epsilon - 1) \, . \tag{4.25}$$

For a rich n-hexane-air ($\phi = 3.0$) flame that exhibits puffing behavior, the initial density is about 1.2 kg/m^3, the laminar flame speed is roughly 0.04 m/s, and the expansion ratio is around 5.5. From Equation 4.25 the pressure jump across the flame front is about 1×10^{-2} Pa.

In the quasi-steady flow outside the flame, the flow-induced pressure, $(\Delta P)_f$, can also be estimated by considering the maximum velocity ahead of the flame from (4.20)

$$(\Delta P)_f \sim \frac{1}{2} \rho u^2 \sim \frac{1}{2} \rho_u (\epsilon - 1)^2 S_l^2 \tag{4.26}$$

which using the values from above is ~ 0.02 Pa.

In comparison to the pressure jump across the flame front and the flow induced pressure, the pressure difference due to gravity across a 10-cm-diameter flame is

$$\Delta P = \rho g d = 1.2 \frac{\text{kg}}{\text{m}^3} \cdot 9.81 \frac{\text{m}}{\text{s}^2} \cdot 0.1 \text{m} = 1.2 \text{ Pa} \, . \tag{4.27}$$

The fact that the hydrostatic pressure head dominates the flame and flow-induced pressure gradients is very relevant to the subsequent discussion on the sources of vorticity at the flame front. It also points out the very substantial role the buoyancy-driven flow will play in the flow field, which supports the scaling arguments advanced earlier.

The simulation results provide the instantaneous velocity vectors created by the expanding flame front. In the lab frame, as shown in Figure 4.10 (a), the flow outside the flame appears to rotates about a point that translates a the puffing cycle progresses [7]. The appearance of rotation and the location of this point is a function of the reference frame chosen. A more detailed analysis of the flow field shows that the trajectory of the fluid elements outside the flame result in complex trajectories due to the competing effects of displacement and entrainment.

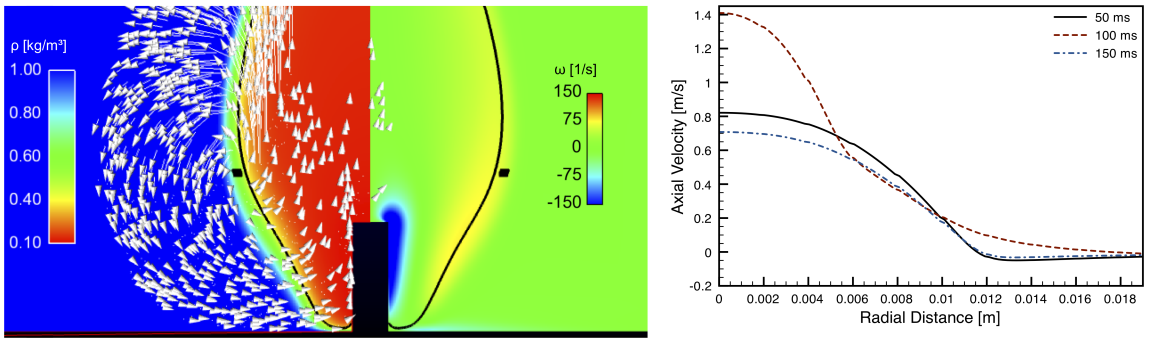

(a) Flow field at 150 ms (b) Axial velocity 20 mm above stagnation surface

Figure 4.10: Flow field and axial velocity at 150 ms (height of glow plug is 11 mm)

Buoyancy accelerates the burned gases upward. If we estimate the resulting velocity, V, after one puffing cycle ($T = 0.1$ seconds)

$$V \sim gT \sim 9.81 \frac{\mathrm{m}}{\mathrm{s}^2} \cdot 0.1\mathrm{s} \sim 1 \frac{\mathrm{m}}{\mathrm{s}} \, . \tag{4.28}$$

This velocity is on the same order of magnitude as the velocities observed in the center of the flame, Figure 4.10 (b).

The vorticity equation is derived by taking the curl of the Navier-Stokes equation and can be expressed as follows:

$$\frac{\partial \omega}{\partial t} + (\mathbf{u} \cdot \nabla)\, \omega = (\omega \cdot \nabla)\, \mathbf{u} - \omega\, (\nabla \cdot \mathbf{u}) + \frac{1}{\rho^2} \left[\nabla \rho \times \nabla p\right] + \nu \nabla^2 \omega \, . \tag{4.29}$$

[7] The location of the center of apparent rotation is identified using a technique similar to Graftieaux et al. (2001).

The first term on the right hand side corresponds to vorticity production due to vortex stretching; the second term arises due to volumetric expansion; the third term is vorticity generation due to baroclinic torque; and the final term is viscous diffusion. The source term due to diffusion gives a length scale outside of the flame that is small, on the order of the flame thickness. The pressure field in Equation 4.29 is obtained from simulation results includes hydrodynamic and hydrostatic effects and can be expressed as

$$\nabla p = \nabla p^{'} + \rho_a g \ . \tag{4.30}$$

We now compute the magnitude of the different source terms in Equation 4.29 using the simulation results for a "puffing" flame at an equivalence ratio of $\phi = 2.5$. It is to be noted that, since the simulations are axisymmetric, only one component of vorticity (which points out of the plane of the paper) is generated.

Figure 4.11 shows a time-instance of the puffing motion with contours for the following terms from left to right: source term due to vortex stretching, source term due to volumetric expansion, source term due to baroclinic torque, sum of all the source terms, and the magnitude of induced vorticity. As before, the flame location is indicated by a black line corresponding to an iso-contour of the progress variable. The contour plot for vorticity includes velocity vectors illustrating the direction of the flow. The source term due to diffusion is small and not plotted here.

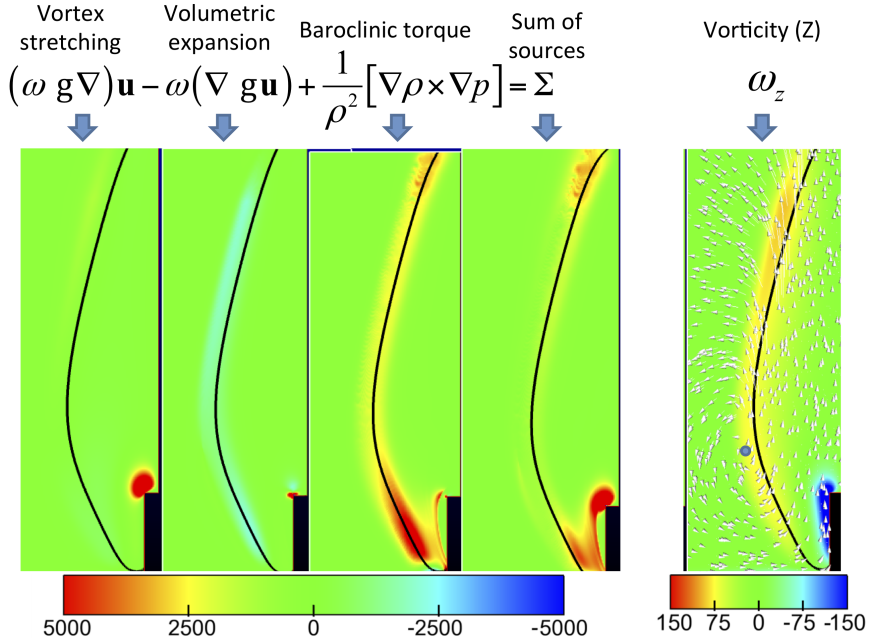

Figure 4.11: The vorticity production terms along the flame front and resulting vorticity at t = 50 ms

The vorticity is primarily generated along the flame front. The source terms due to vortex stretching and volumetric expansion along the flame front are opposite in direction to that produced by baroclinic torque. In case of baroclinic torque, the source term is seen to be primarily concentrated along the vertical sections of the flame front. The magnitude of this term is also seen to be considerably larger (100 times) than that due to vortex stretching and volumetric expansion. The net result is a positive (counter clockwise) generation of vorticity along the vertical edges of the flame.

Figure 4.12 shows contours of three quantities: density gradient, pressure gradient, and resulting baroclinic torque as well as the vorticity. The directions of the density and pressure gradients are further illustrated by arrows.

The location along the flame front where vorticity is generated (primarily due to baroclinic torque as shown in Fig. 4.11) is coincident with a large density and pressure gradient. These gradients are seen to be almost perpendicular to each other with the density gradient pointing mostly horizontally away from the flame front and the pressure gradient pointing predominantly vertically downwards.

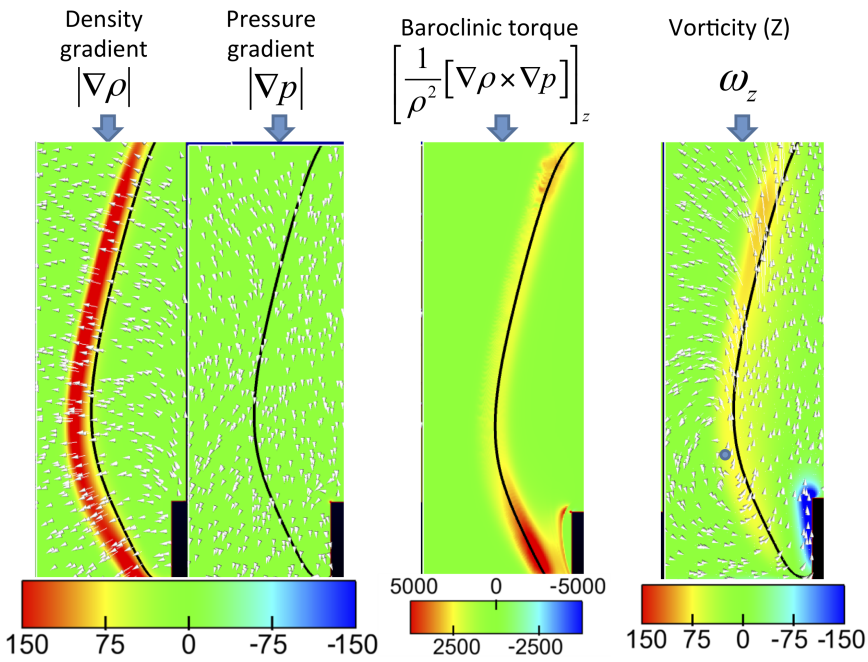

Figure 4.12: Gradients of density, pressure and the resulting baroclinic torque and overall vorticity along the flamefront at t = 50 ms associated with the incipient puff

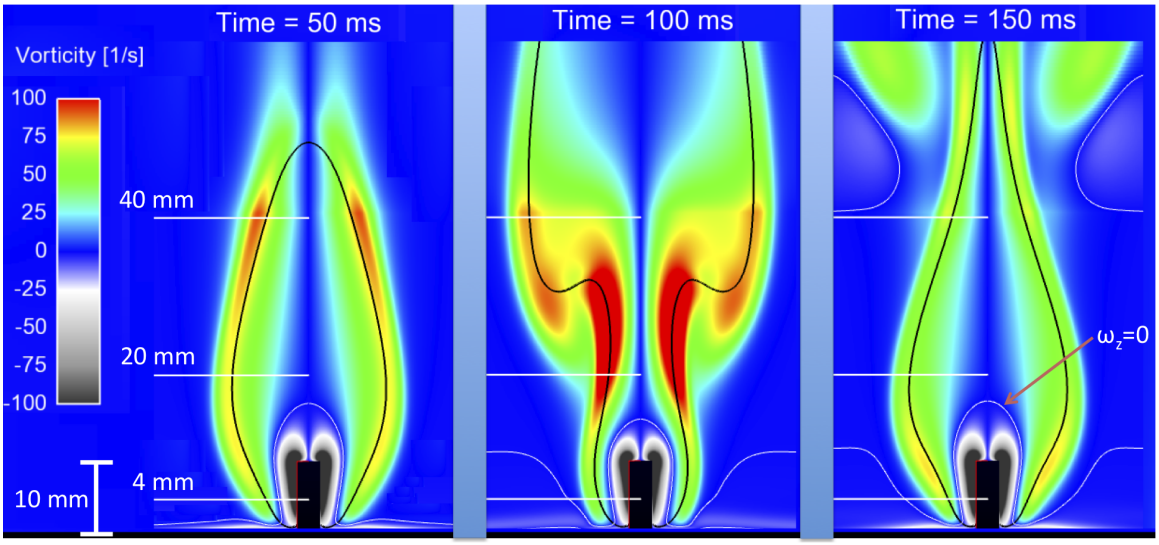

Figure 4.13: Detailed vorticity distribution at simulation time of 50, 100, and 150 ms (zero vorticity contour is indicated by the thin white line); subsequent figures show density, vorticity, and velocity profiles at the indicated locations 4, 20, and 40 mm above the stagnation surface

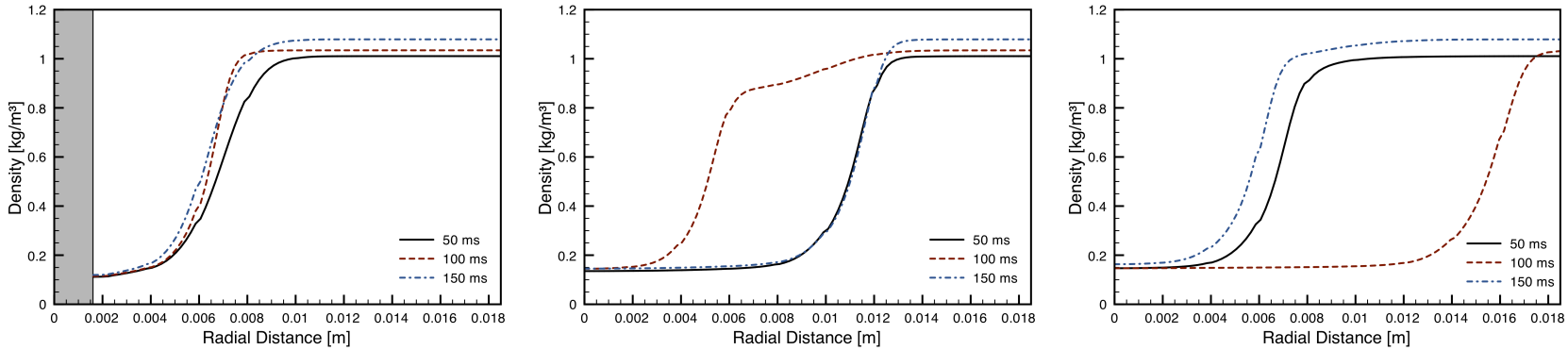

(a) 4 mm above stagnation surface (b) 20 mm above stagnation surface (c) 40 mm above stagnation surface

Figure 4.14: Density as a function of radial location at different locations in the flame

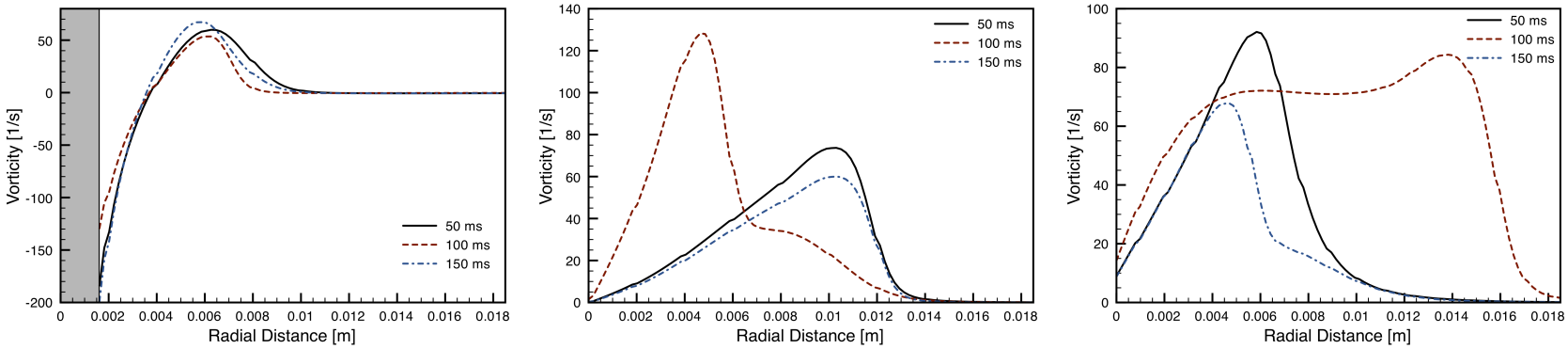

(a) 4 mm above stagnation surface (b) 20 mm above stagnation surface (c) 40 mm above stagnation surface

Figure 4.15: Vorticity as a function of radial location at different locations in the flame

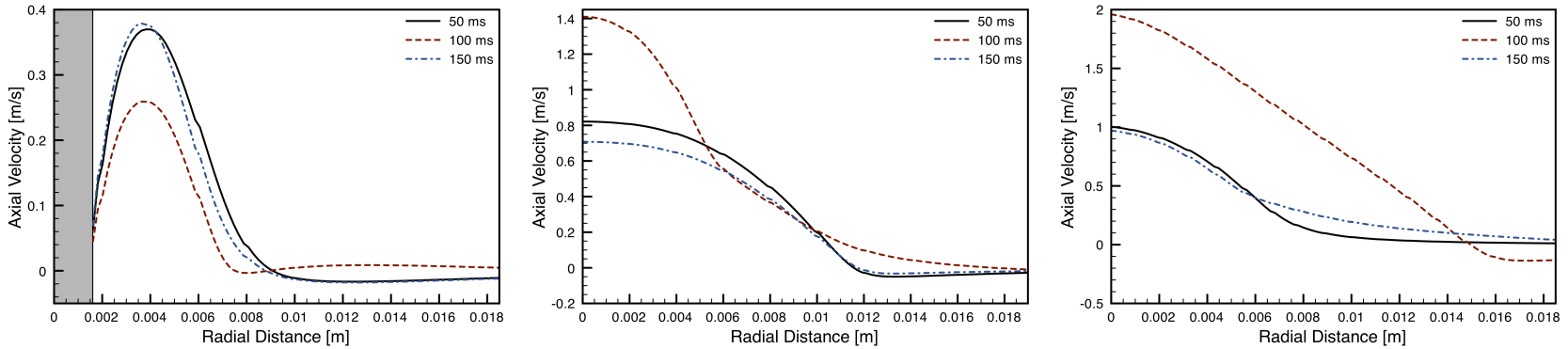

(a) 4 mm above stagnation surface (b) 20 mm above stagnation surface (c) 40 mm above stagnation surface

Figure 4.16: Axial velocity as a function of radial location at different locations in the flame

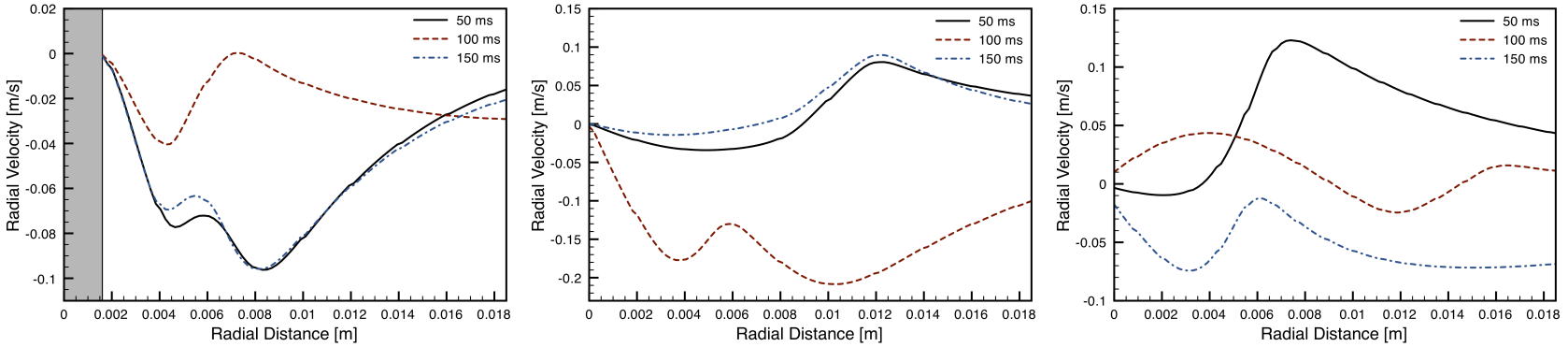

(a) 4 mm above stagnation surface (b) 20 mm above stagnation surface (c) 40 mm above stagnation surface

Figure 4.17: Radial velocity as a function of radial location at different locations in the flame

The vorticity generated at the flame front can also be estimated following the work of Uberoi et al. (1958). The analysis of Uberoi et al. (1958) can extended to include the effect of gravity to obtain the vorticity downstream of an irrotational flow

$$u_n\omega_\theta = -\frac{1}{\rho}\frac{\partial P}{\partial s} - \frac{1}{2}\frac{\partial}{\partial s}\left(u_n^2 + u_t^2\right) + g_t \tag{4.31}$$

where u_n is the velocity normal to the flame front, u_t is the velocity tangential to the flame front, ω_θ is vorticity out of the page, s is the coordinate along the flame front, and g_t is the component of gravity tangential to the flame front. Using the momentum and mass balance across the flame front as in Uberoi et al. (1958), the vorticity inside the flame can be shown to be

$$\omega_{\theta f} = \frac{\rho_b - \rho_u}{\rho u_n}\vec{g}\cdot\vec{t} = \frac{\rho_b - \rho_u}{\rho_u S_l}g_t \approx \left(\frac{1}{\epsilon} - 1\right)\frac{g}{S_l} \approx 200 \text{ s}^{-1} \tag{4.32}$$

This estimate is consistent with the results obtained in the simulations, which can be seen particularly clearly in Figures 4.15 and 4.13 as well as the analysis in Emmons (1958).

The velocity that is then induced by a vorticity distribution can be calculated using the Biot-Savart law (Batchelor, 2007)

$$\vec{u} = -\frac{1}{4\pi}\int \frac{\vec{s}\times\vec{\omega}(\zeta)}{s^3}dV_\zeta \ . \tag{4.33}$$

For a cylindrical sheet of vorticity $dV_\zeta = 2\pi r dr dz$ and along the centerline $s = \sqrt{r^2 + (z - z_0)^2}$.

If we consider a finite sheet of vorticity of length L, that only extends over the flame front δ_f for a flame or radius R,

$$u = -\frac{1}{4\pi}\int_{-L/2}^{L/2}\int_{R}^{R+\delta_f}\frac{\omega_\theta \sin\theta}{s^2}2\pi r dr dz \tag{4.34}$$

where $\sin\theta = r/s$.

$$u = -\frac{1}{4\pi}\int_{-L/2}^{L/2}\int_{R}^{R+\delta_f}\frac{\omega_\theta r}{s^3}2\pi r dr dz \tag{4.35}$$

Since the flame is thin relative to the flame radius, i.e., $\delta_f \ll R$,

$$u = -\frac{1}{4\pi}\int_{-L/2}^{L/2}\int_{R}^{R+\delta_f}\frac{\omega_\theta r}{\left(R^2 + (z - z_0^2)\right)^{3/2}}2\pi r dr dz \ . \tag{4.36}$$

This allows us to integrate in r

$$u = -\frac{2\pi\omega_\theta}{4\pi}\int_{-L/2}^{L/2}\frac{1}{\left(R^2 + (z - z_0^2)\right)^{3/2}}dz\int_{R}^{R+\delta_f} r^2 dr \ . \tag{4.37}$$

Once again because $\delta_f \ll R$, the second integral can be approximated as $R^2\delta_f$

$$u = -\frac{2\pi\omega_\theta R^2\delta_f}{4\pi}\int_{-L/2}^{L/2}\frac{1}{\left(R^2+(z-z_0)^2\right)^{3/2}}dz\ , \tag{4.38}$$

which for $z_0 = 0$ becomes

$$u = -\frac{2\pi\omega_\theta\delta_f}{4\pi}\left[\frac{z}{\left(R^2+z^2\right)^{1/2}}\right]_{-L/2}^{L/2} \tag{4.39}$$

$$u = -\frac{2\pi\omega_\theta\delta_f}{4\pi}\frac{L}{\left(R^2+L^2/4\right)^{1/2}}\ , \tag{4.40}$$

$$u = -\omega_\theta\delta_f\frac{L}{\left(4R^2+L^2\right)^{1/2}}\ , \tag{4.41}$$

For a flame of 10 mm radius and with a 40 mm height the final inflow velocity using the 200 s^{-1} vorticity is 0.18 m/s, which is about 15 - 20% of the velocity observed inside the flame (see Figure 4.16).

Therefore the main mechanism responsible for creating the inflow ultimately leading to the formation of a "puff" is buoyancy with a lesser contribution from flame-generated vorticity.

4.4.2 Onset of Puffing — Flow Velocity vs. Flame Velocity

The flow velocity and flame velocity can be extracted directly from the simulation. In Figures 4.18 and 4.19, both are presented as a function of the coordinate along the flame front, arclength, starting at the base of the flame at the glow plug and ending at the top of the flame. Figure 4.18 shows the evolution of the flame propagation speed at various instances in time. The flame speed is strongly influenced by the temperature and flow velocity in the hot plume above the glow plug, which increase the flame speed. As the flame propagates out of the plume, the propagation speed asymptotes to a constant value comparable to the product of the laminar burning velocity, S_L, and the expansion ratio across the flame front, ϵ, $V_f = \epsilon S_L$.

The inflow velocity is computed by taking the negative of the normal component of the flow velocity ($-\vec{u}\cdot\hat{n}$) along the flame front. Initially, the flame pushes the gases outward giving a negative inflow velocity as shown in Figure 4.19. The flow then turns inward and gains in magnitude. This increase in inflow velocity is due to the entrainment of the buoyant plume of combustion products and the continuous production of vorticity along the flame front due to the baroclinic torque.

At 50 ms, the inflow velocity exceeds the flame propagation velocity (Fig. 4.20). At this point, the flame moves back towards the centerline. This is because the flame motion is relative to the

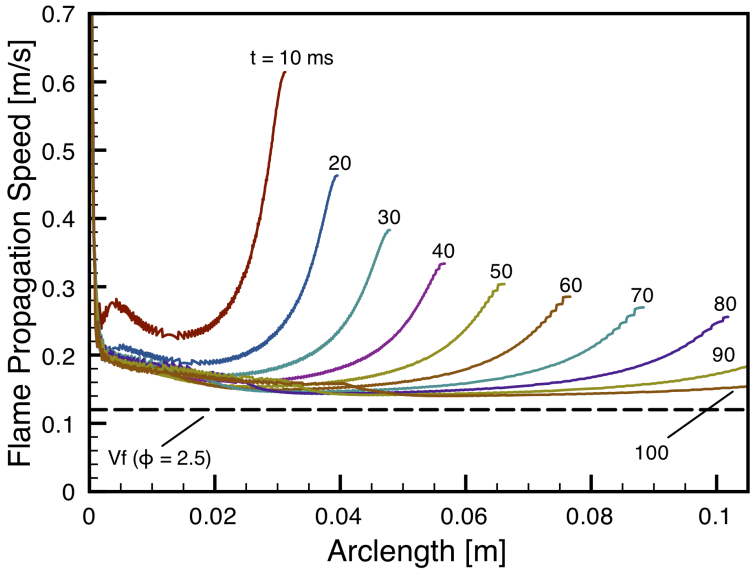

Figure 4.18: Flame propagation speed along the the flame front as a function of time

incoming flow. After this point on in the puffing cycle, the inflow velocity will be greater than the burning speed until the puffing cycle is complete. Figure 4.20 shows a direct comparison of the flame propagation and flow velocity indicating the crossover point between 40 ms and 50 ms and between 140 ms and 150 ms (100 ms later). This analysis also shows the origin of the puffing frequency at 10 Hz. The inflow must be strong enough to exceed flame propagation to generate the periodic motion. The puff is advected sufficiently fast that the subsequent puff is its own independent event where entrainment flow is gathered and not influenced by the previous cycle.

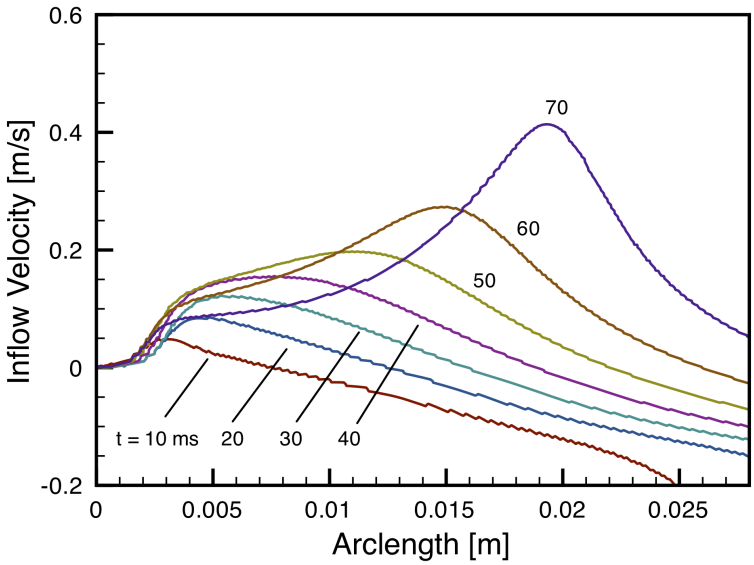

Figure 4.19: Inflow velocity along the the flame front as a function of time. Positive velocities mean flow going from unburned to burned side.

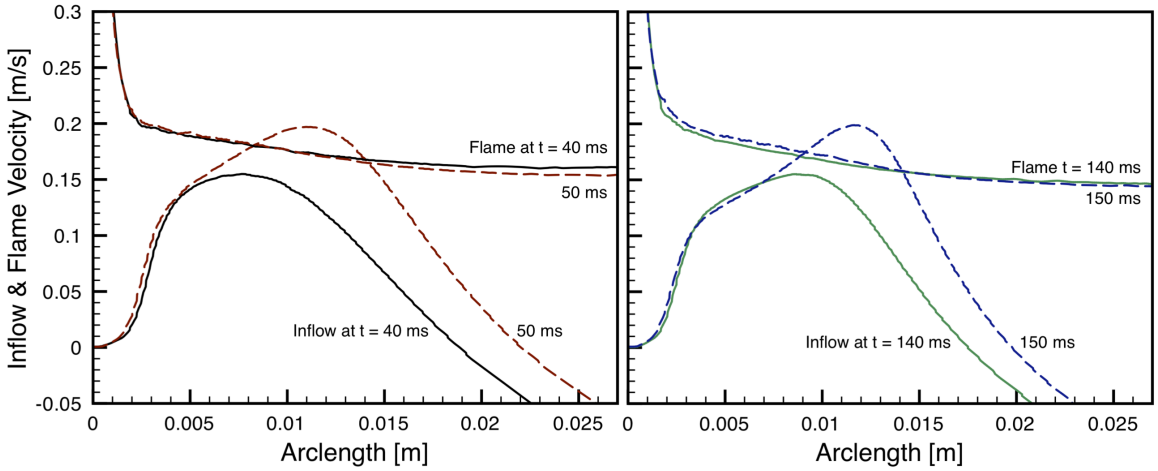

Figure 4.20: Inflow velocity and flame propagation velocity along the the flame front as a function of time showing the 10 Hz frequency observed in experiments and simulations

4.5 Conclusions

In experiments of hot surface ignition and subsequent flame propagation a ∼10 Hz puffing flame is visible in mixtures that are stagnant and premixed prior to the ignition sequence. This discovery extends the range of observed puffing or flickering flames that were previously observed in non-premixed flame and premixed injection flames. By varying the size of the hot surface, power input, and combustion vessel volume, we determined that the periodic motion is a function of the interaction of the flame with the fluid flow induced by the combustion products rather than the initial plume established by the hot surface. Additionally, the periodic motion is neither caused by acoustic interaction with the vessel nor by a large-scale recirculation zone. The phenomenon is accurately reproduced in numerical simulations and a detailed flow field analysis revealed a competition between the inflow velocity at the base of the flame and the flame propagation speed. The inflow is caused by the entrainment flow due the buoyancy acceleration of the light combustion products and the vorticity generated at the flame front. The increasing inflow velocity, which exceeds the flame propagation speed is ultimately responsible for creating a "puff", which is the accelerated upward, a process that is then repeated periodically until the combustion vessel is filled with products sufficiently to interrupt the process.

Chapter 5

Conclusions

In this work, thermal ignition has been investigated for homogeneously heated mixtures that expand our knowledge of auto-ignition as well as heterogeneously heated mixtures that show how hot surfaces interact with flammable mixtures as well as the subsequent flame propagation.

The auto-ignition experiment was constructed to allow for precise control of the mixture composition as well as temperature history, while simultaneously allowing for measurements of the fuel concentration in addition to temperature and pressure measurements. The experimental results showed that the rate at which the mixture is heated to the expected auto-ignition temperature played an important role. Mixtures heated sufficiently slowly can undergo a slow reaction that does not lead to a explosion event. Fast heating rates initiate an ignition event that is associated with rapid consumption of the fuel and a substantial pressure rise. The transition between these two events can be produced by varying the heating rate by as little as a factor of 2 in the experiments.

Detailed and simplified chemistry models were used to confirm these observations in the context of the classical Semenov thermal ignition theory. The detailed chemistry showed that the chemical pathways differ depending on the heating rate. During slow heating, peroxides are formed that react slowly, while in fast heating case chain branching occurs that results in rapid energy release. The simplified chemistry model was successfully used to pinpoint the effect the heating rate in transitioning a mixture evolution from a slow reaction to an ignition. While the heating rate is acknowledged as a factor in the literature, this detailed study underlines the importance of considering the heating rate in safety testing and design.

The hot surface ignition experiments highlight the increased temperature necessary to ignite flammable mixtures that are heated by an isolated hot surface. The ignition temperature shows a dependence on mixture composition and initial pressure. The ignition temperature is modeled to varying degrees of sophistication including the balance between diffusion time scale and ignition

time scale, to considering the trajectories of fluid elements and their temperature evolution along a vertical hot plate, and finally using tabulated detailed chemistry in a full fluid mechanics simulation. All models show reasonable agreement with the experiment away from the rich and lean extremes and an increasing level of applicability with increasing sophistication.

The flame propagation that follows the ignition is investigated over a range of mixture compositions leading to a range of flame propagation speeds. The measured propagation speed is consistent with numerical simulations and literature data. As the propagation speed decreases with increasing fuel concentration above slightly more than stoichiometric, the flame is more and more dominated by buoyancy effects. This competition between the flame propagation and buoyancy appears to be characterized appropriately by a Richardson number. As the Richardson number reaches unity, lifting flames and subsequent re-ignition at the glow plug is observed, and further increase in Richardson number results in puffing flames.

The puffing flame phenomenon is investigated by a detailed analysis of the flow field. The flow field is extracted from the simulation results and shows an inflow at the bottom of the flame due to buoyancy and vorticity generated at the flame front. Baroclinic torque is identified as the main source of vorticity, which is due to the misalignment of the density gradient across the flame front and the hydrostatic pressure gradient. The puffing motion is initiated because the inflow velocity exceeds the flame propagation speed. The puff is then accelerated upward leading to a decay in the inflow velocity so that the flame can again expand and the process repeats itself.

In summary the following observations were made in this study:

1. auto-ignition depends on the heating rate and can results in either a slow or fast reaction
2. A dramatic change in explosion behavior occurs with small changes in heating rate
3. Hot surface ignition temperature is insensitive to composition away from the limits
4. A new premixed combustion mode is observed for the first time: premixed puffing flames

Bibliography

J. Adler. Ignition of a combustible stagnant gas layer by a circular hot-spot. *Combustion Theory and Modelling*, 3(2):359–369, 1999. *Cited on page: 75.*

J. Adler and J. W. Enig. The critical conditions in thermal explosion theory with reactant consumption. *Combustion and Flame*, 8(2):97–103, 1964. *Cited on pages: 54 and 56.*

ASTM. ASTM E659-78 (2005) Standard Test Method for Autoignition Temperature of Liquid Chemicals, 2005. *Cited on pages: xiii, 2, 4, 7, 8, 13, and 95.*

ASTM. ASTM D56-05 (2010) Standard Test Method for Flash Point by Tag Closed Cup Tester, 2010. *Cited on pages: 2 and 8.*

V. Babrauskas. *Ignition Handbook*. Fire Science Publishers, 2003. *Cited on pages: 3, 4, 5, 6, and 9.*

H. C. Bailey and R. G. W. Norrish. The oxidation of hexane in the cool-flame region. *Proceedings of the Royal Society of London*, 212(1110):311–330, 1952. *Cited on page: 7.*

S. P. M. Bane. Personal Communication, 2011. *Cited on page: 127.*

S. P. M. Bane, J. L. Ziegler, P. A. Boettcher, S. A. Coronel, and J. E. Shepherd. Experimental investigation of spark ignition energy in kerosene, hexane, and hydrogen. *Journal of Loss Prevention in the Process Industries*, 2011. *Cited on page: 1.*

G. K. Batchelor. *An Introduction to Fluid Dynamics*. Cambridge University Press, 2007. *Cited on page: 138.*

M. J. Bennett. Ignition of combustible fluids by heated surfaces. *Process safety progress*, 20(1): 29–36, 2001. *Cited on page: 10.*

G. Blanquart. Personal Communication, 2011. *Cited on pages: 105, 106, and 191.*

G. Blanquart, P. Pepiot-Desjardins, and H. Pitsch. Chemical mechanism for high temperature combustion of engine relevant fuels with emphasis on soot precursors. *Combustion and Flame*, 156(3):588–607, 2009. *Cited on pages: 90 and 103.*

P. A. Boettcher, R. Mével, V. Thomas, and J. E. Shepherd. The effect of heating rates on low temperature hexane air combustion. *Fuel*, 2011. *Cited on page: 201.*

P. N. Brown, G. D. Byrne, and A. C. Hindmarsh. Vode, a variable-coefficient ode solver. *The SIAM Journal on Scientific and Statistical Computing*, 10:1038–1051, 1989. *Cited on page: 23.*

J. Buckmaster and N. Peters. The infinite candle and its stability–a paradigm for flickering diffusion flames. In *Symposium (International) on Combustion*, volume 21, pages 1829–1836. Elsevier, 1988. *Cited on pages: 11 and 115.*

A. Burcat, E. Olchanski, and C. Sokolinski. Kinetics of hexane combustion in a shock tube. *Israel Journal of Chemistry*, 36:313–320, 1996. *Cited on pages: 23, 24, 25, and 43.*

L. R. Cairnie and A. J. Harrison. Natural convection adjacent to a vertical isothermal hot plate with a high surface-to-ambient temperature difference. *International Journal of Heat and Mass Transfer*, 25(7):925–934, 1982. *Cited on pages: xvi, 81, 88, and 90.*

B. M. Cetegen and T. A. Ahmed. Experiments on the periodic instability of buoyant plumes and pool fires. *Combustion and Flame*, 93(1–2):157–184, 1993. *Cited on pages: x, 11, 115, 121, 122, 123, 125, and 126.*

D. S. Chamberlin and A. Rose. The flicker of luminous flames. *Proceedings of the Symposium on Combustion*, 1:27–32, 1948. *Cited on pages: 10 and 115.*

R. K. Cheng, B. Bédat, and L. W. Kostiuk. Effects of buoyancy on lean premixed V-flames Part I: laminar and turbulent flame structures. *Combustion and flame*, 116(3):360–375, 1999. *Cited on pages: 11 and 115.*

J. D. Colwell and A. Reza. Hot Surface Ignition of Automotive and Aviation Fluids. *Fire Technology*, 41:105–123, 2005. *Cited on pages: 2, 7, 10, and 13.*

H. F. Coward and P. G. Guest. Ignition of natural gas-air mixtures by heated metal bars 1. *Journal of the American Chemical Society*, 49(10):2479–2486, 1927. *Cited on pages: 3 and 8.*

Coordinating Research Council CRC. *Handbook of Aviation Fuel Properties—CRC Report No. 530.* Society of Automotive Engineers, Warrendale, PA, 1983. *Cited on pages: xxvi, 2, 7, and 13.*

H. J. Curran, P. Gaffuri, W. J. Pitz, C. K. Westbrook, and W. R. Leppard. Autoignition chemistry of the hexane isomers: an experimental and kinetic modelling study. In *SAE International Fuels and Lubricants Meeting and Exposition*, 1995. *Cited on page: 23.*

H. J. Curran, P. Gaffuri, W. J. Pitz, and C. K. Westbrook. A comprehensive modeling study of n-heptane oxidation. *Combustion and flame*, 114(1–2):149–177, 1998. *Cited on pages: xvi, 84, 85, and 93.*

P. Dagaut, M. Reuillon, and M. Cathonnet. Experimental study of the oxidation of n-heptane in a jet stirred reactor from low to high temperature and pressures up to 40 atm. *Combustion and Flame*, 101:132–140, 1995. *Cited on pages: 24 and 25.*

S. G. Davis and C. K. Law. Laminar flame speeds and oxidation kinetics of iso-octane-air and n-heptane-air flames. *Twenty-Seventh Sysposium (International) on Combustion*, 27(1):521–527, 1998a. *Cited on pages: 90 and 103.*

S. G. Davis and C. K. Law. Determination of and fuel structure effects on laminar flame speeds of C1 to C8 hydrocarbons. *Combustion Science and Technology*, 140(1-6):427–449, 1998b. *Cited on pages: 103, 104, 105, 106, 191, 192, 194, and 195.*

H. Davy. Some new experiments and observations on the combustion of gaseous mixtures, with an account of a method of preserving a continued light in mixtures of inflammable gases and air without flame. *Philosophical Transactions of the Royal Society of London*, 107:77–85, 1817. *Cited on page: 3.*

O. Desjardins, G. Blanquart, G. Balarac, and H. Pitsch. High order conservative finite difference scheme for variable density low mach number turbulent flows. *Journal of Computational Physics*, 227(15):7125–7159, 2008. *Cited on pages: 91 and 102.*

J. A. Drallmeier. Hydrocarbon absorption coefficients at the 3.39-μm He-Ne laser transition. *Applied Optics*, 42(6):979–982, 2003. *Cited on pages: 14, 15, and 165.*

D. F. G. Durao and J. H. Whitelaw. Instantaneous velocity and temperature measurements in oscillating diffusion flames. *Proceedings of the Royal Society of London. A. Mathematical and Physical Sciences*, 338(1615):479, 1974. *Cited on pages: 11 and 115.*

D. Durox, F. Baillot, P. Scouflaire, and R. Prud'Homme. Some effects of gravity on the behaviour of premixed flames. *Combustion and Flame*, 82(1):66–74, 1990. *Cited on pages: 11 and 115.*

D. Durox, T. Yuan, and E. Villermaux. The effect of buoyancy on flickering in diffusion flames. *Combustion Science and Technology*, 124(1–6):277–294, 1996. *Cited on pages: x, 11, 123, and 124.*

H. W. Emmons. *Fundamentals of Gas Dynamics*, volume 3. Princeton University Press Princeton, 1958. Section G - Gas Dynamics of Combustion and Detonations. Chapter 2 - Flow Discontinuities Associated with Combustion. *Cited on page: 138.*

D. A. Frank-Kamenetskii. *Diffusion and heat transmission in chemical kinetics*. Plenum, New York, 1969. *Cited on pages: 46, 47, 178, and 187.*

A. G. Gaydon and H. G. Wolfhard. *Flames*. Chapman and Hall, 4th edition, 1979. *Cited on pages: 105 and 125.*

B. Gebhart, Y. Jaluria, R.L. Mahajan, and B. Sammakia. *Buoyancy-induced flows and transport*. Hemisphere Publishing, New York, NY, 1988. *Cited on pages: 81, 82, and 85.*

I. Glassman. *Combustion*. Academic Press, San Diego, 4th edition, 2008. *Cited on pages: 5, 6, 43, 46, 48, 50, 75, 99, and 108.*

D. G. Goodwin. An open-source, extensible software suite for chemical vapor deposition process simulation. *Chemical Vapor Deposition XVI and EUROCVD*, 14:2003–08, 2003. *Cited on pages: 23, 43, 69, and 70.*

S. Gordon and B. J. McBride. Computer program for calculation of complex chemical equilibrium compositions and applications. Technical report, National Aeronautics and Space Administration, Office of Management, Scientific and Technical Information Program, 1994. *Cited on page: 201.*

L. Graftieaux, M. Michard, and N. Grosjean. Combining piv, pod and vortex identification algorithms for the study of unsteady turbulent swirling flows. *Measurement Science and technology*, 12:1422, 2001. *Cited on page: 132.*

A. J. Grant and J. M. Jones. Low-frequency diffusion flame oscillations. *Combustion and Flame*, 25:153–160, 1975. *Cited on pages: 11 and 115.*

B. F. Gray. The dependence of spontaneous ignition temperature on surface to volume ratio in static systems for fuels showing a negative temperature coefficient. *Combustion and Flame*, 14 (1):113–115, 1970. *Cited on page: 8.*

J. F. Griffiths, P. A. Halford-Maw, and D. J. Rose. Fundamental Features of Hydrocarbon Autoignition in a Rapid Compression Machine. *Combustion and Flame*, 95(3):291–306, 1993. *Cited on page: 7.*

Y. T. Guahk, D. K. Lee, K. C. Oh, and H. D. Shin. Flame-intrinsic kelvin- helmholtz instability of flickering premixed flames. *Energy & Fuels*, 23(8):3875–3884, 2009. *Cited on pages: 11, 12, and 115.*

T. J. Held, A. J. Marchese, and F. L. Dryer. A semi-empirical reaction mechanism for n-heptane oxidation and pyrolysis. *Combustion Science and Technology*, 123:107–146, 1997. *Cited on pages: 24 and 25.*

C. E. Hermance. Implications concerning general ignition processes from the analysis of homogeneous, thermal explosions. *Combustion Science and Technology*, 10(5):261–265, 1975. *Cited on pages: 55 and 56.*

K. M. Hinckley and A. J. Dean. Time resolved measurements of fuelair stoichiometry in pulse detonation engines using a non-intrusive laser sensor. *43rd AIAA Aerospace Sciences Meeting and Exhibition paper number AIAA 2005-0628*, 2005. *Cited on page: 165.*

Y. Huang, C. J. Sung, and J. A. Eng. Laminar flame speeds of primary reference fuels and reformer gas mixtures. *Combustion and Flame*, 139(3):239–251, 2004. *Cited on pages: 103, 105, and 106.*

D. N. Jaynes and B. H. Beam. Hydrocarbon gas absorption by a He-Ne laser beam at a 3.39 μm wavelength. *Applied Optics*, 8(8):1741–1742, 1969. *Cited on pages: 15 and 165.*

C. Ji, E. Dames, Y. L. Wang, H. Wang, and F. N. Egolfopoulos. Propagation and extinction of premixed C_5–C_{12} *n*-alkane flames. *Combustion and Flame*, 157(2):277–287, 2010. *Cited on pages: 99, 103, 105, 106, 193, and 195.*

K. Kadoya, N. Matsunaga, and A. Nagashima. *Viscosity and thermal conductivity of dry air in the gaseous phase.* American Chemical Society and the American Institute of Physics for the National Bureau of Standards, 1985. *Cited on page: 85.*

G. P. Kane, E. A. C. Chamberlain, and D. T. A. Townend. The Spontaneous Ignition under Pressure of the Simpler Aliphatic Hydrocarbons, Alcohols, and Aldehydes. *Journal of Chemical Society*, pages 436–443, 1937. *Cited on pages: xiv, 35, and 36.*

M. Kaviany. *Principles of heat transfer.* Wiley, New York, NY, 2002. *Cited on pages: 80 and 82.*

R. J. Kee, M. E. Coltrin, and P. Glarborg. *Chemically reacting flow: theory and practice*. John Wiley and Sons, 2003. *Cited on page: 79.*

A. P. Kelley, A. J. Smallbone, D. L. Zhu, and C. K. Law. Laminar flame speeds of C5 to C8 n-alkanes at elevated pressures: Experimental determination, fuel similarity, and stretch sensitivity. *Proceedings of the Combustion Institute*, 33:963–970, 2011. *Cited on pages: 23, 99, 103, 105, 106, 125, 191, 193, and 195.*

I. Kimura. Stability of Laminar Jet Flames. *Tenth Symposium (International) on Combustion*, pages 1295–1300, 1965. *Cited on pages: 11 and 115.*

A. E. Klingbeil, J. B. Jeffries, and R. K. Hanson. Temperature- and pressure-dependent absorption cross sections of gaseous hydrocarbons at 3.39 μm. *Measurements Science and Technology*, 17: 1950–1957, 2006. *Cited on pages: 14, 15, and 165.*

L. W. Kostiuk and R. K. Cheng. The coupling of conical wrinkled laminar flames with gravity. *Combustion and flame*, 103(1–2):27–40, 1995. *Cited on page: 115.*

M. Kroll, J. A. McClintock, and O. Ollinger. Measurement of gaseous oxygen using diode laser spectroscopy. *Applied Physics Letters*, 51:1465–1467, 1987. *Cited on page: 19.*

J. M. Kuchta. Investigation of Fire and Explosion Accidents in the Chemical, Mining, and Fuel-Related Industries. Bulletin 680, Bureau of Mines, 1985. *Cited on pages: xxvi, 7, and 13.*

J. M. Kuchta, A. Bartkowiak, and M. G. Zabetakis. Hot surface ignition temperatures of hydrocarbon fuel vapor-air mixtures. *Journal of Chemical and Engineering Data*, 10(3):282–288, 1965. *Cited on pages: xiii, 3, 5, 8, 9, 13, 75, 94, 95, 96, 185, 187, and 188.*

K. Kumar, J. E. Freeh, C. J. Sung, and Y. Huang. Laminar flame speeds of preheated iso-octane/O_2/N_2 and n-heptane/O_2/N_2 mixtures. *Journal of propulsion and power*, 23(2):428–436, 2007. *Cited on pages: 103, 105, and 106.*

R. K. Kumar. Ignition of hydrogen-oxygen-diluent mixtures adjacent to a hot, nonreactive surface. *Combustion and flame*, 75(2):197–215, 1989. *Cited on pages: 9 and 75.*

N. M. Laurendeau. Thermal ignition of methane-air mixtures by hot surfaces: A critical examination. *Combustion and Flame*, 46:29–49, 1982. *Cited on pages: 8, 9, 75, 76, 78, 94, and 186.*

C. K. Law. *Combustion physics*. Cambridge University Press, 2006. *Cited on pages: xv, 48, 50, 51, and 181.*

C. K. Law and H. K. Law. Thermal-ignition analysis in boundary-layer flows. *Journal of Fluid Mechanics*, 92(01):97–108, 1979. *Cited on pages: 78 and 87.*

B. Lewis. *Selected Combustion Problems*, page 177. Butterworths Scientific Publications, 1954. *Cited on page: 125.*

X. D. Liu, S. Osher, and T. Chan. Weighted essentially non-oscillatory schemes. *Journal of Computational Physics*, 115(1):200–212, 1994. *Cited on page: 91.*

J. Luque and D. R. Crosley. Lifbase: Database and spectral simulation (version 2.0. 60, 2008). Technical report, Tech. rep., SRI International, 1999. *Cited on page: 119.*

W. Mason and R. V. Wheeler. CCXLIX—The ignition of gases. Part II. Ignition by a heated surface. Mixtures of methane and air. *J. Chem. Soc., Trans.*, 121:2079–2091, 1922. *Cited on page: 7.*

MATLAB. *version 7.9.0.529 (R2009b)*. The MathWorks Inc., Natick, Massachusetts, 2010. *Cited on page: 203.*

S. K. Menon. Personal Communication, 2011. *Cited on page: 121.*

R. Mével, F. Lafosse, N. Chaumeix, G. Dupré, and C.-E. Paillard. Spherical expanding flames in H_2-N_2O-Ar mixtures: flame speed measurements and kinetic modeling. *International Journal of Hydrogen Energy*, 34:9007–9018, 2009. *Cited on page: 101.*

R. Mével, P. A. Boettcher, and J. E. Shepherd. Absorption Cross Section at 3.39 μm of Alkanes, Aromatics and Substituted Hydrocarbons. *Chem Phys Lett, submitted for publication*, 2012. *Cited on pages: 15 and 165.*

K. Narayanaswamy, G. Blanquart, and H. Pitsch. A consistent chemical mechanism for oxidation of substituted aromatic species. *Combustion and Flame*, 157(10):1879–1898, 2010. *Cited on pages: 90 and 103.*

NFPA 325. *Guide to Fire Hazard Properties of Flammable Liquids, Gases, and Volatile Solids.* National Fire Protection Association, Quincy, MA, 1994. *Cited on page: 2.*

NTSB. In-flight Breakup Over The Atlantic Ocean, Trans World Airlines Flight 800, Boeing 747-131, N93119, Near East Moriches, New York, July 17, 1996. Technical report, National Transportation Safety Board, Washington, DC, 2000. *Cited on page: 1.*

S. Ono, H. Kawano, H. Niho, and G. Fukuyama. Ignition in a Free Convection from Vertical hot Plate. *Bulletin of the JSME-Japan Society of Mechanical Engineers*, 19(132):676–683, 1976. *Cited on page: 8.*

M. Parang and M. C. Jischke. Adiabatic ignition of homogeneous systems. *AIAA Journal*, 13: 405–408, 1975. *Cited on pages: 55 and 56.*

M. Y. Perrin and J. M. Hartmann. High-Temperature Absorption of the 3.39 μm He-Ne Laser Line by Methane. *Journal of Quantitative Spectroscopy & Radiative Transfer*, 42(6):459–464, 1989. *Cited on page: 165.*

L. C. Philippe and R. K. Hanson. Laser diode wavelength-modulation spectroscopy for simultaneous measurement of temperature, pressure, and velocity in shock-heated oxygen flows. *Applied Optics*, 32:6090–6103, 1993. *Cited on page: 19.*

M. J. Pilling, editor. *Comprehensive Chemical Kinetics* , chapter 6 by J. F. Griffiths and C. Mohamed — Experimental and Numerical Studies of Oxidation Chemistry and Spontaneous Ignition Phenomena, pages 545–650. Elsevier, 1997. *Cited on pages: 5, 7, and 13.*

H. Pitsch and M. Bollig. Flamemaster, a computer code for homogeneous and one-dimensional laminar flame calculations. *Institut für Technische Mechanik, RWTH Aachen*, 1994. *Cited on pages: 84, 103, and 191.*

M. I. Radulescu and B. M. Maxwell. Critical ignition in rapidly expanding self-similar flows. *Physics of Fluids*, 22:066101, 2010. *Cited on page: 54.*

H. P. Ramirez, K. Hadj-Ali, P. Dievart, G. Dayma, C. Togbe, G. Moreac, and P. Dagaut. Oxidation of commercial and surrogate bio-diesel fuels (B30) in a jet-stirred reactor at elevated pressure: Experimental and modeling kinetic study. *Proceedings of the Combustion Institute*, 33:375–382, 2011. *Cited on pages: xxvi, 23, 104, 194, 196, and 201.*

J. Reid and D. Labrie. Second Harmonic Detection with Tunable Diode Lasers Comparison of Experiment and Theory. *Applied Physics*, 26:203–210, 1981. *Cited on page: 167.*

R. C. Reid, J. M. Prausnitz, and B. E. Poling. *The properties of gases and liquids.* McGraw Hill Book Co., New York, NY, 3rd edition, 1977. *Cited on page: 68.*

M. Ribaucour, R. Minetti, M. Carlier, and L. R. Sochet. Autoignition at High-Pressure — Design, Construction and Test of a Rapid Compression Machine. *Journal de Chimie Phsique et de Physico-Chimie Biologique*, 89(11–12):2127–2152, 1992. *Cited on page: 7.*

G. B. Rieker. Personal Communication, 2009. *Cited on page: 171.*

G. B. Rieker, J. B. Jeffries, and R. K. Hanson. Calibration-free wavelength-modulation spectroscopy for measurements of gas temperature and concentration in harsh environments. *Applied Optics*, 48(29):5546–5560, 2009. *Cited on pages: 19, 171, and 172.*

L. S. Rothman, D. Jacquemart, A. Barbe, D. C. Benner, M. Birk, L. R. Brown, M. R. Carleer, C. Chackerian, K. Chance, L. H. Coudert, V. Dana, V. M. Devi, J. M. Flaud, R. R. Gamache, A. Goldman, J. M. Hartmann, K. W. Jucks, A. G. Maki, J. Y. Mandin, S. T. Massie, J. Orphal, A. Perrin, C. P. Rinsland, M. A. H. Smith, J. Tennyson, R. N. Tolchenov, R. A. Toth, J. Vander Auwera, P. Varanasi, and G. Wagner. The HITRAN 2004 molecular spectroscopic database. *Journal of Quantitative Spectroscopy & Radiative Transfer*, 96(2):139–204, 2005. *Cited on page: 165.*

G. S. Scott, G. W. Jones, and F. E. Scott. Determination of Ignition Temperatures of Combustible Liquids and Gases. *Analytical Chemistry*, 20(3):238–241, 1948. *Cited on page: 3.*

N. N. Semenov. Thermal theory of combustion and explosion. *Progress of Physical Science*, 23, 1940. English Version: Technical Memorandums - National Committee for Aeronautics No.-1024 (NACA 1024). *Cited on pages: 4, 13, 21, 42, 46, 50, 75, 78, 94, 181, 185, 186, 187, and 188.*

G. S. Settles. *Schlieren and shadowgraph techniques: visualizing phenomena in transparent media.* Springer Verlag, 2001. *Cited on page: 64.*

S. W. Sharpe, T. J. Johnson, R. L. Sams, P. M. Chu, G. C. Rhoderick, and P. A. Johnson. Gas-phase databases for quantitative infrared spectroscopy. *Applied Spectroscopy*, 58(12):1452–1461, DEC 2004. ISSN 0003-7028. *Cited on page: 165.*

H. P. S. Shen, J. Steinberg, J. Vanderover, and M. A. Oehlschlaeger. A shock tube study of the ignition of n-heptane, n-decane, n-dodecane, and n-tetradecane at elevated pressures. *Energy & Fuels*, 23(5):2482–2489, 2009. *Cited on pages: 84, 90, and 103.*

I. G. Shepherd, R. K. Cheng, and M. S. Day. The dynamics of flame flicker in conical premixed flames: An experimental and numerical study. Technical report, Lawrence Berkeley National Laboratory Report LBNL-59249, 2005. *Cited on pages: 11, 12, and 115.*

J. E. Shepherd. Personal Communication, 2012. *Cited on page: 9.*

J. E. Shepherd and A. C. Ratzel. Heat transfer resulting from premixed combustion. *Heat Transfer in Fire and Combustion Systems, ASME HTD-45*, pages 191–201, 1985. *Cited on page: 69.*

J. E. Shepherd, C. J. Krok, and J. J. Lee. Spark Ignition Energy Measurements in Jet A. Technical report, Graduate Aeronautical Laboratories at the California Institute of Technology, Pasadena, CA, 1997. *Cited on page: 1.*

J. E. Shepherd, C. D. Nuyt, and J. J. Lee. Flash Point and Chemical Composition of Aviation Kerosene (Jet A). Technical report, Graduate Aeronautical Laboratories at the California Institute of Technology, Pasadena, CA, 1999. *Cited on pages: 1 and 7.*

J. E. Shepherd, S. Browne, and J. Ziegler. Numerical Solution Methods for Shock and Detonation Jump Conditions. Technical report, Aeronautical and Mechanical Engineering California Institute of Technology, Pasadena, CA, 2006. *Cited on page: 201.*

J. Simmie. Detailed chemical kinetic models for the combustion of hydrocarbon fuels. *Progress in Energy and Combustion Science*, 29:599–634, 2003. *Cited on page: 23.*

K. C. Smyth and N. P. Bryner. Short-duration autoignition temperature measurements for hydrocarbon fuels near heated metal surfaces. *Combustion Science and Technology*, 126(1–6):225–253, 1997. *Cited on pages: 8, 9, 95, and 96.*

K. Stephan and A. Laesecke. *The thermal conductivity of fluid air*. American Chemical Society and the American Institute of Physics for the National Bureau of Standards, 1985. *Cited on page: 85.*

K. Stewartson. *The theory of laminar boundary layers in compressible fluids*. Oxford University Press, 1964. *Cited on page: 81.*

A. Strawa and B. Cantwell. Investigation of an excited jet diffusion flame at elevated pressure. *Journal of Fluid Mechanics*, 200:309–336, 1989. *Cited on pages: 11 and 115.*

K. Tanoue, Y. Ogura, M. Takayanagi, and T. Nishimura. Measurement of temperature distribution for the flickering phenomenon around the premixed flame by using laser speckle method. *Journal of visualization*, 13(3):183–185, 2010. *Cited on pages: 11, 12, and 115.*

Teledyne Judson Technologies. J14 Series Lead Selenide Detectors Product Bulletin, Oct 2000. URL http://www.teledynejudson.com/files/pdf/selenide_PB3326.pdf. *Cited on page: 162.*

W. M. Thornton. LX. The ignition of gases by hot wires. *Philosophical Magazine Series 6*, 38(227): 613–633, 1919. *Cited on page: 3.*

E. Tomita, N. Kawahara, M. Shigenaga, A. Nishiyama, and R. W. Dibble. In situ measurement of hydrocarbon fuel concentration near a spark plug in an engine cylinder using the 3.392 μm infrared laser absorption method: discussion of applicability with a homogeneous methane/air mixture. *Measurement Science and Technology*, 14(8):1350, 2003. *Cited on page: 165.*

T. Toong, R. F. Salant, J. M. Stopford, and G. Y. Anderson. Mechanisms of combustion instability. *Tenth Symposium (International) on Combustion*, pages 1301–1313, 1965. *Cited on pages: 11 and 115.*

D. T. A. Townend, L. L. Cohen, and M. R. Mandlekar. The influence of pressure on the spontaneous ignition of inflammable gas-air mixtures. iii. hexane-and isobutane-air mixtures. *Proceedings of the Royal Society of London. Series A*, 146(856):113–129, 1934. *Cited on pages: xiii and 6.*

D. J. Tritton. *Physical Fluid Dynamics*. Oxford University Press, New York, 1988. *Cited on pages: 8 and 197.*

T. Tsuboi, K. Inomata, Y. Tsunoda, A. Isobe, and K. Nagaya. Light-absorption by hydrocarbon molecules at 3.392 μm of He-Ne Laser. *Japanese Journal of Applied Physics Part 1 - Regular Papers Short Notes & Review Papers*, 24(1):8–13, 1985. *Cited on pages: 15 and 165.*

M. S. Uberoi, A. M. Kuethe, and H. R. Menkes. Flow field of a bunsen flame. *Physics of Fluids*, 1 (2):150–158, 1958. *Cited on page: 138.*

J. P. J. Van Lipzig, E. J. K. Nilsson, L. P. H. De Goey, and A. A. Konnov. Laminar burning velocities of n-heptane, iso-octane, ethanol and their binary and tertiary mixtures. *Fuel*, 2011. *Cited on pages: 103, 105, and 106.*

G. Vanhove, G. Petit, and R. Minetti. Experimental study of the kinetic interactions in the low-temperature autoignition of hydrocarbon binary mixtures and a surrogate fuel. *Combustion and Flame*, 145(3):521–532, 2006. *Cited on page: 7.*

W. G. Vincenti and C. H. Kruger. *Introduction to physical gas dynamics*. Krieger Publishing Company, 1967. *Cited on page: 183.*

H. Wang, E. Dames, B. Sirjean, D. A. Sheen, R. Tangko, A. Violi, J. Y. W. Lai, F. N. Egolfopoulos, D. F. Davidson, R. K. Hanson, C. T. Bowman, C. K. Law, W. Tsang, N. P. Cernansky, D. L.

Miller, and R. P. Lindstedt. A high-temperature chemical kinetic model of n-alkane (up to n-dodecane), cyclohexane, and methyl-, ethyl-, n-propyl and n-butyl-cyclohexane oxidation at high temperatures, JetSurF version 2.0, September 19, 2010., 2010. URL (http://melchior.usc.edu/JetSurF/JetSurF2.0). *Cited on page: 192.*

J. Warnatz, U. Maas, and R.W. Dibble. *Combustion: Physical and Chemical Fundamentals, Modeling and Simulation, Experiments, Pollutant Formation.* Springer Verlag, 2006. *Cited on page: 6.*

C. K. Westbrook and F. L. Dryer. Chemical Kinetics Modeling of Hydrocarbon Combustion. *Progress in Energy and Combustion Science*, 10(1):1–57, 1984. *Cited on page: 43.*

C. K. Westbrook, W. J. Pitz, O. Herbinet, H. J. Curran, and E. J. Silke. A comprehensive detailed chemical kinetic reaction mechanism for combustion of n-alkane hydrocarbons from n-octane to n-hexadecane. *Combustion and Flame*, 156(1):181–199, 2009. *Cited on pages: 84, 90, and 103.*

F. M. White. *Heat Transfer.* Addison-Wesley, Boston, MA, 1984. *Cited on page: 26.*

R. G. White. Spontaneous ignition of kerosene/AVTUR/vapour — the effect of the ratio, vessel surface area to volume (effect of vessel surface area on minimum spontaneous ignition temperature of kerosene). Technical report, Royal Aircraft Establishment 67107, 1967. *Cited on page: 8.*

R. D. Wilk, N. P. Cernansky, and R. S. Cohen. The Oxidation of Propane at Low and Transition Temperatures. *Comb. Sci. and Tech*, 49:41–78, 1986. *Cited on page: 7.*

C. H. Yang and B. F. Gray. Slow oxidation of hydrocarbons and cool flames. *The Journal of Physical Chemistry*, 73(10):3395–3406, 1969. *Cited on page: 6.*

S. Yoshiyama, Y. Hamamoto, E. Tomita, and K. Minami. Measurement of hydrocarbon fuel concentration by means of infrared absorption technique with 3.39 μm He-Ne laser. *JSAE Rev.*, 17: 339–345, 1996. *Cited on page: 165.*

M. G. Zabetakis. Flammability characteristics of combustible gases and vapors. Technical report, Bureau of Mines, 1965. Bulletin 627. *Cited on pages: 68, 74, and 127.*

M. G. Zabetakis, A. L. Furno, and G. W. Jones. Minimum spontaneous ignition temperatures of combustibles in air. *Industrial & Engineering Chemistry*, 46(10):2173–2178, 1954. *Cited on page: 3.*

V. P. Zhukov, V. A. Sechenov, and A. Yu. Starikovskii. Ignition delay times in lean n-hexane-air mixture at high pressures. *Combustion and Flame*, 136:257–259, 2004. *Cited on pages: 23, 24, and 25.*

E. E. Zukoski. Fluid dynamic aspects of room fires. In *Proc. of First International Symp. Fire Safety Science*, 1986. *Cited on pages: 11 and 115.*

This page intentionally left blank.